Measurements from the *RV Ronald H. Brown* and related platforms as part of the Atlantic Tradewind Ocean-Atmosphere Mesoscale Interaction Campaign (ATOMIC)

Patricia K. Quinn[1], Elizabeth J. Thompson[2], Derek J. Coffman[1], Sunil Baidar[3,4], Ludovic Bariteau[2], Timothy S. Bates[1,5], Sebastien Bigorre[6], Alan Brewer[4], Gijs de Boer[2,3], Simon P. de Szoeke[7], Kyla Drushka[8], Gregory R. Foltz[9], Janet Intrieri[2], Suneil Iyer[8], Chris W. Fairall[2], Cassandra J. Gaston[10], Friedhelm Jansen[11], James E. Johnson[1,5], Ovid O. Krüger[12], Richard D. Marchbanks[3,4], Kenneth P. Moran[2,3], David Noone[13], Sergio Pezoa[2], Robert Pincus[2,3], Albert J. Plueddemann[6], Mira L. Pöhlker[12], Ulrich Pöschl[12], Estefania Quinones Melendez[7], Haley M. Royer[10], Malgorzata Szczodrak[10], Jim Thomson[8], Lucia M. Upchurch[1,5], Chidong Zhang[1], Dongxiao Zhang[1,5], and Paquita Zuidema[10]

[1] NOAA Pacific Marine Environmental Laboratory (PMEL), Seattle, WA, USA
[2] NOAA Physical Sciences Laboratory (PSL), Boulder, CO, USA
[3] Cooperative Institute for Research in Environmental Sciences (CIRES), University of Colorado, Boulder, CO
[4] NOAA Chemical Sciences Laboratory (CSL), Boulder, CO, USA
[5] Cooperative Institute for Climate Ocean and Ecosystem Studies (CICOES), University of Washington, Seattle, WA, USA
[6] Woods Hole Oceanographic Institution (WHOI), Woods Hole, MA, USA
[7] Oregon State University, Corvallis, OR, USA
[8] University of Washington, Applied Physics Laboratory (APL), Seattle, WA
[9] NOAA Atlantic Oceanographic and Meteorological Laboratory (AOML), Miami, FL, USA
[10] Rosenstiel School of Marine and Atmospheric Science, University of Miami, Miami, FL, USA
[11] Max Planck Institute for Meteorology, Hamburg, Germany
[12] Max Planck Institute for Chemistry, Mainz, Germany
[13] University of Auckland, Auckland, NZ

Correspondence: Patricia K. Quinn (patricia.k.quinn@noaa.gov)

Abstract. The Atlantic Tradewind Ocean-Atmosphere Mesoscale Interaction Campaign (ATOMIC) took place from January 7 to July 11, 2020 in the tropical North Atlantic between the eastern edge of Barbados and 51°W, the longitude of the Northwest Tropical Atlantic Station (NTAS) mooring. Measurements were made to gather information on shallow atmospheric convection, the effects of aerosols and clouds on the ocean surface energy budget, and mesoscale oceanic processes. Multiple platforms were deployed during ATOMIC including the *NOAA RV Ronald H. Brown* (RHB) (Jan. 7 to Feb. 13) and WP-3D Orion (P-3) aircraft (Jan. 17 to Feb. 10), the University of Colorado's Robust Autonomous Aerial Vehicle – Endurant and Nimble (RAAVEN) Uncrewed Aerial System (UAS) (Jan. 24 to Feb. 15), NOAA- and NASA-sponsored Saildrones (Jan. 12 to Jul. 11), and Surface Velocity Program Salinity (SVPS) surface ocean drifters (Jan. 23 to Apr. 29). The *RV Ronald H. Brown* conducted *in situ* and remote sensing measurements of oceanic and atmospheric properties with an emphasis on mesoscale oceanic-atmospheric coupling and aerosol-cloud interactions. In addition, the ship served as a launching pad for Wave Gliders, Surface Wave Instrument Floats with Tracking (SWIFTs), and radiosondes. Details of measurements made from the *RV Ronald H. Brown*, ship-deployed assets, and other platforms closely coordinated with the ship during ATOMIC are provided here. These platforms include Saildrone 1064 and the RAAVEN UAS as well as the

Barbados Cloud Observatory (BCO) and Barbados Atmospheric Chemistry Observatory (BACO). Inter-platform comparisons are presented to assess consistency in the data sets. Data sets from the *RV Ronald H. Brown* and deployed assets have been quality controlled and are publicly available at the NOAA Physical Sciences Laboratory (PSL) ATOMIC ftp server (ftp://ftp2.psl.noaa.gov/Projects/ATOMIC/data/ (Quinn et al., 2020)). In addition, the data have been submitted to NOAA's National Centers for Environmental Information (NCEI) data archive (https://www.ncei.noaa.gov/) for Digital Object Identifiers (DOIs). Point of contact information and links to individual data sets are provided herein.

1. Introduction

Shallow, liquid clouds persist at altitudes of hundreds to a few thousand meters above most of the world's oceans. Convection and mixing in the boundary layer can lead to the formation of shallow clouds, which can drive more mixing throughout the cloud layer and result in deeper convection. These clouds reflect incoming solar radiation and lead to a cooling of the surface (Vial et al., 2016). In addition, shallow mixing influences sea surface temperature (SST) and salinity by moderating the air-sea exchanges of energy and moisture (Stevens et al., 2016). Climate models have difficulty accurately representing low clouds in trade-wind regions because many of the processes involved in their formation occur at sub-grid scales (Bony et al., 2015). Improving model performance requires measurements that will result in a better understanding of 1) the boundary layer conditions that lead to cloudiness, 2) the influence of clouds and the atmospheric boundary layer on the upper ocean mixed layer, and in turn, 3) the influence of ocean mixing processes on surface fluxes and the atmospheric boundary layer.

ATOMIC took place in the boreal winter to study shallow convection and low, liquid clouds at a time of year when other cloud types are mostly absent. ATOMIC is the U.S. complement to the Elucidating the Role of Clouds Circulation Coupling in Climate Campaign (EUREC[4]A) (Bony et al., 2017;Stevens et al., 2020). Together, ATOMIC and EUREC[4]A involved 4 research vessels, 4 research aircraft, land-based observations from Barbados, and uncrewed sea-going and aerial vehicles. The ATOMIC - EUREC[4]A study region stretched from the eastern shores of Barbados to the NTAS buoy located ~500 NM to the northeast and south along the coast of South America to ~ 5°N. EUREC[4]A platforms focused on the western portion of the study area while the *RV Ronald H. Brown* and P-3 aircraft worked primarily in the eastern, upwind sector from mid-January to mid-February (Fig. 1). ATOMIC was composed of two legs with Leg 1 conducted between Jan. 7 and 25, 2020 and Leg 2 conducted between Jan. 28 and Feb.13, 2020. NOAA- and NASA-sponsored Saildrones covered the entire study area between January and July 2020. The RAAVEN UAS flew near shore from Morgan Lewis on the eastern side of Barbados between January 24 and February 15. SVPS type surface ocean drifters were deployed from the *RV L'Atalante* and operated along the South American coast (Jan. 23 to Apr. 29).

Figure 1. Tracks of the *RV Ronald H. Brown*, Wave Gliders, and SWIFTS during ATOMIC (colored by seawater skin T calculated by PSL) for a) Leg 1 and b) Leg 2. Tracks for Wave Gliders, and SWIFTS are magnified in c) Leg 1 and d) Leg 2. The portion of the EUREC⁴A study area overlapping with ATOMIC is indicated by the solid green line in b). Locations of *RV Ronald H. Brown* stations, MOVE, and BCO/BACO are also shown in a) and b).
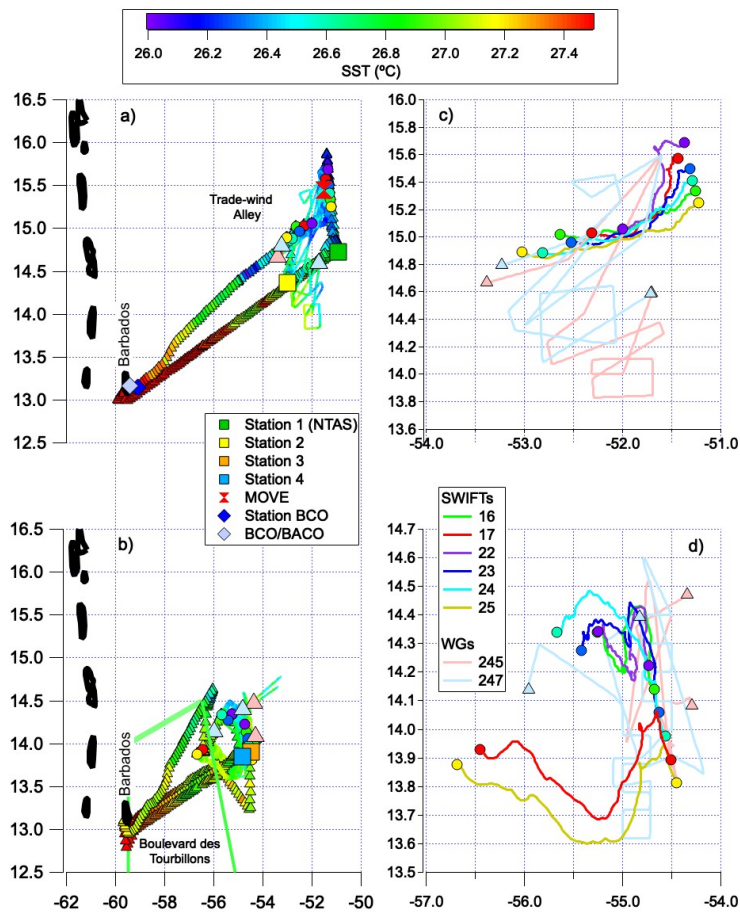
A thorough description of the objectives of ATOMIC and first highlights of the data analyses are presented in Zuidema (2020). A description of data collected from the P-3 is described in Pincus et al. (2020) and data collected by the RAAVEN are documented in de Boer et al. (2020). Here, a detailed overview of the data collected from the *RV Ronald H. Brown* and deployed assets is provided. The goal is to document the sampling strategy,

100 instrumentation used, and data availability to advance the widespread use of the data by the ATOMIC and broader
101 research communities. A description of the sampling strategy, including coordination with other platforms, is
102 described in Sect. 2. Also detailed in Sect. 2 are the measurements made from the *RV Ronald H. Brown,* the NTAS
103 moored buoy, Wave Gliders and SWIFT vessels, Saildrones, RAAVEN UAS, and SVPS drifters. An overview of
104 oceanic and atmospheric conditions sampled is provided in Sect. 3. Results from inter-platform comparisons of
105 atmospheric and oceanic parameters are detailed in Sect. 4. Data availability, format, and quality control are
106 described in Sect. 5 along with links to individual data sets. Available measurement uncertainties are reported in the
107 data set metadata at ftp://ftp2.psl.noaa.gov/Projects/ATOMIC/data/ and https://www.ncei.noaa.gov/.
108
109 **2. Sampling strategy and measurements**
110
111 Sampling onboard the *RV Ronald H. Brown* took place from Jan. 7 to Feb. 13, 2020 and focused on the region
112 between 57°W and 51°W east of Barbados and between 13° and 16°N in the so-called Trade Wind Alley (Fig. 1).
113 The overarching strategy of ATOMIC was to provide a view of the atmospheric and oceanic conditions upwind of
114 the EUREC^{4}A study region. Operations of the *RV Ronald H. Brown* were coordinated with the Wave Gliders and
115 SWIFTs deployed from the ship, the P-3 aircraft, Saildrone 1064, and BCO and BACO. An additional logistical
116 objective included recovering the NTAS-17 mooring and replacing it with the NTAS-18 mooring. A third objective
117 was to triangulate and download data from a Meridional Overturning Variability Experiment (MOVE) subsurface
118 mooring and related Pressure Inverted Echo Sounders (PIES). MOVE is designed to monitor the integrated deep
119 meridional flow in the tropical North Atlantic.
120
121 Optimal aerosol and flux measurements were made when the ship was pointed into the wind to avoid contamination
122 by the ship's stack and air flow distortion. Coordinating with the P-3 and Saildrone and deploying the NTAS
123 Mooring, Wave Gliders, and SWIFTs had the advantage of providing redundant and complimentary data streams but
124 the disadvantage of requiring the ship to transit away from the wind for maneuvers. In addition, ship transits to
125 Bridgetown, Barbados for a scheduled in port (Jan. 26 to 28) and a medical emergency (Feb. 3 to 6) were downwind
126 relative to prevailing northeast trade winds. Periods of unfavorable winds for atmospheric sampling were identified
127 by relative winds from behind the ship's beam (~ - 90° through 180° to + 90° relative to the bow at 0°). A time
128 series of relative winds and corresponding high particle number concentrations due to emissions from the ship's
129 stack (~> 1000 cm^{-3}) is shown in Figure 2. These periods have been removed from the aerosol data. Unfavorable
130 sampling conditions were experienced 15% of the time the ship was at sea at the dates and times indicated in Table
131 1. Seawater measurements were less accurate when the ship's speed over water was near zero due to mechanical
132 stirring of the water surface by the ship's propulsion system.
133
134 A general timeline of events for Legs 1 and 2 is provided in Sect. 2.1. and 2.2. Descriptions of the instrumentation
135 onboard the ship and deployed assets are provided in Sect. 2.3 to 2.7 and on the Saildrone, RAAVEN UAS, and
136 SVPS drifters in Sect. 2.8 to 2.10.

Figure 2. Time series of relative wind direction (apparent wind relative to the bow of the ship, negative values are port and positive values are starboard) and particle number concentration $(D_{gn} > 13\ nm)$ measured on the *RV Ronald H. Brown* during ATOMIC.
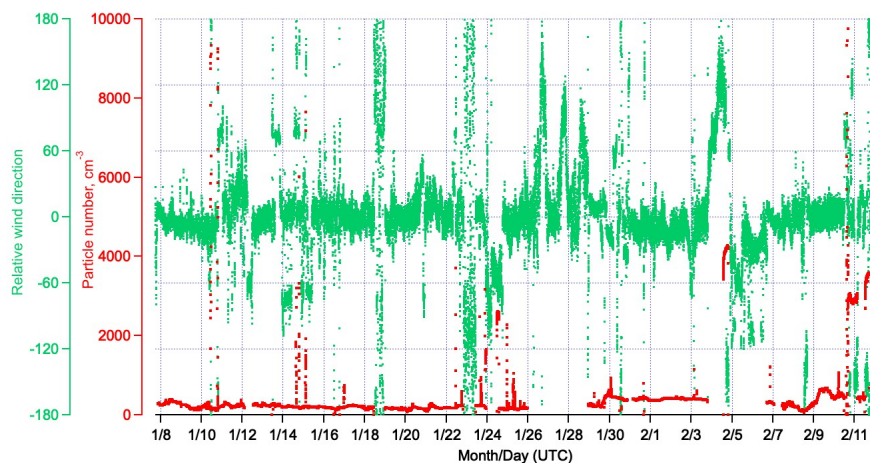
2.1. Sampling events during Leg 1

Timeline of events for Legs 1 and 2 are shown in Table 1. Dates and positions of deployment and recovery of assets are listed in Table 2. Times when platforms were within relatively close proximity providing the potential for inter-platform comparisons are given in Table 3. All times reported throughout the paper are in UTC.

During Leg 1, the NTAS mooring was swapped out, Wave Gliders were deployed for the duration of the experiment, and the SWIFTs were deployed and then recovered at the end of the leg. In addition to these logistical operations, measurements were made throughout the leg to characterize atmospheric and oceanic conditions upwind of the EUREC⁴A study region.

The ship departed Bridgetown, Barbados on Jan. 7, 2020 in transit to the NTAS-18 mooring target location at 14°44'N and 50°56'W. Radiosonde launches every 4 hours and continuous atmosphere and sea surface sampling began early on Jan. 8. The latitude and longitude of the four stations occupied during the cruise are listed in Table 1 and shown in Figure 1. Station 1 (S1) was located in the NTAS region. Two Wave Gliders were deployed on Jan. 9 *en route* to S1. Once at S1, early on Jan. 10 a comparison between shipboard and NTAS-17 atmosphere and ocean measurements was conducted. The NTAS-18 mooring was deployed later on Jan. 10. After deployment, the ship transited 55 NM to the northwest of S1 to the MOVE region near 15°27'N and 51°32'W (Figure 1). Unsuccessful

Deleted: ¶
¶
¶
¶

166 attempts were made over a 24 hr period to triangulate the position of the MOVE1-13 mooring and PIES198 and 238.

167 The ship left the MOVE region on Jan. 12 at 05:30 to transit back to S1. The MOVE work did not compromise

168 continuous atmospheric and surface ocean sampling and is not discussed further.

169

170 **Table 1.** Timeline of sampling events onboard the *RV Ronald H. Brown* (RHB) including coordination with other
171 platforms, NTAS operations, downwind transits, and periods on Station. The different colors shown under RHB
172 correspond to the status of the ship. *NTAS-18 deployed. **NTAS-17 recovered.
173

	Sampling days
	Downwind transit
	In port
	NTAS Operations
	MOVE Operations
C-BCO	Comparison with BCO
C-P3 (Research Flight number)	Coordination with P3
C-SD	Comparison with SailDrone 1064
C-S	Comparison with SWIFTs
C-N17	Comparison with NTAS 17
C-N18	Comparison with NTAS 18
C-RUAS	Comparison with RAAVEN UAS
S1	Station 1 14°44' N, 50°56'W (NTAS area)
S2	Station 2 14º21'44"N, 53ºW
S3	Station 3 13º54'N, 54º30'W
S4	Station 4 13º51'N, 54º51'36"W
Station BCO	Station BCO 13º8'55.7", 59º4'59.2"W

174

	RHB	SWIFTs	WG 245	WG 247	CTD	uCTD	NTAS/MOVE
Jan 7							
8							
9	S1						
10	S1, C-N17						N18*
11							MOVE
12	S1, C-N18						
13	S1, C-N18, C-S						
14	C-S						
15	S1, C-N17						
16	S1, C-N17						N17**
17	S1, C-P3(RF1)						
18	C-P3 (RF2)						
19	S2						
20	S2						
21	S2						
22	C-S						
23	C-P3(RF3)						
24	C-BCO, C-RUAS						
25	C-BCO, C-RUAS						
26							
27							
28							
29							
30	C-S, S3						
31	S3, C-P3(RF5)						
Feb 1	S3						
2	S3						
3	S3, C-P3(RF6)						
4							
5							
6							
7							
8	S4, C-SD, C-P3(RF9)						

9	S4, C-SD							
10	S4, C-SD, C-P3(RF10)							
11	C-S, C-WG, C-P3(RF11)							
12								
13								

179

180 **Table 2.** Dates (UTC) and positions of deployment and recovery of NTAS moorings, two Wave Gliders, and six
181 SWIFTs. Assets are listed in order of start and stop times of the data stream. Distance travelled is given for the
182 SWIFTs and Wave Gliders.

| Asset | Deployment | | Recovery | | Distance (NM) |
	Date	Position	Date	Position	
LEG 1					
Wave Glider 245	1/9/20 20:55	14° 35' 25" N, 51° 41' 56" W			
Wave Glider 247	1/9/20 20:55	14° 35' 13" N, 51° 42' 21" W			
NTAS-18	1/10/20 17:45	14° 44' N, 50° 56'W			
SWIFT 22	1/14/20 01:13	15° 41' 21" N, 51° 22' 5" W	1/22/20 19:14	15° 3' 29" N, 51° 59' 50" W	52
SWIFT 23	1/14/20 05:11	15° 29' 59" N, 51° 18' 54" W	1/22/20 15:11	14° 57' 47" N, 52° 31' 21" W	62
SWIFT 24	1/14/20 07:11	15° 24' 42" N, 51° 17' 19" W	1/22/20 12:13	14° 53' 12" N, 52° 49' 5" W	94
SWIFT 16	1/14/20 9:11	15° 20' 3" N, 51° 15' 37"	1/22/20 14:13	15° 1' 9", 52° 38' 8"W	82
SWIFT 25	1/14/20 10:12	15° 15' 7" N, 51° 13' 46" W	1/22/20 11:13	14° 53' 26"N, 53° 1' 34" W	60
SWIFT 17	1/14/20 18:11	15° 34' 31" N, 51° 26' 16" W	1/22/20 17:14	15° 1' 55" N, 52° 18' 56" W	60
NTAS-17			1/16/20 10:41	14° 49' 28" N, 51° 00' W	
LEG 2					
Wave Glider 245			2/7 19:55	14° 4' 55" N, 54° 17' 12" W	153
SWIFT 22	1/30/20 17:12	14° 13' 25" N, 54° 43' 53" W	2/10/20 17:12	14° 20' 35" N, 55° 15' 5" W	31
SWIFT 16	1/30/20 18:13	14° 8' 23" N, 54° 40' 51" W	2/10/20 17:13	14° 20' 28" N, 55° 15' 19" W	36
SWIFT 23	1/30/20 19:12	14° 3' 31" N, 54° 37' 30" W	2/10/20 20:15	14° 16' 30" N, 55° 25' 14" W	48
SWIFT 24	1/30/20 20:13	13° 58' 39" N, 54° 33' 52" W	2/10/20 23:12	14° 20' 19" N, 55° 39' 56" W	68
Wave Glider 247			2/11/20 10:54	14° 8' 11" N, 55° 57' 9" W	248
SWIFT 17	1/30/20 21:10	13° 53' 40" N, 54° 30 '31" W	2/11/20 15:11	13° 55' 47" N, 56° 27' 6" W	127
SWIFT 25	1/30/20 22:13	13° 48' 50" N, 54° 27' 6" W	2/11/20 17:14	13° 52' 37" N, 56° 41' 0.6" W	130

183

184 **Table 3.** Times when platforms were within relatively close proximity providing the potential for inter-platform
185 comparisons. Also given are distances between platforms during the comparisons. Results from inter-platform
186 comparisons reported here are indicated in bold. Distances between RHB and NTAS refer to distance to the mooring
187 anchor. Distance to buoys were between 0.25 to 3 NM.

Platforms	Start UTC	Stop UTC	Distance (NM)	Comments
RHB, NTAS-17	1/10/20 00:58	1/10/20 08:57	2.5 (mooring anchor)	Station 1
RHB, NTAS-18	**1/12/20 11:30**	**1/13/20 14:00**	**2.9 (mooring anchor)**	**1/12/20 14:06, 19:04; 1/13/20 00:00** **CTD casts to 250 m** **Station 1**
RHB, NTAS-17	**1/15/20 10:00**	**1/16/20 09:05**	**2.9 (mooring anchor)**	**1/15/20 20:16** **CTD cast to 5000 m** **Station 1**
RHB, P-3	1/17/20 14:20		Within dropsonde circle	P-3 RF1, 7.3 – 7.7 km altitude Station 1
RHB, P-3	1/19/20 14:57		Within dropsonde circle	P-3 RF2 7.6 km altitude Station 2
RHB, P-3	1/23/20 14:06, 19:46		Within dropsonde circle	P-3 RF3, 3.2 km altitude 14° 22' 59"N and 55°W Overfly of ship at 150 m at 15:42
RHB, P-3	1/31/20 16:25		Within dropsonde circle	P-3 RF5, 7.4 km altitude Station 3
RHB, P-3	2/3/20 14:13		Within dropsonde circle	P-3 RF6, 7.7 km altitude Station 3
RHB, P-3	2/9/20 05:57		Within dropsonde circle	P-3 RF9, 7.5 km altitude Station 4
RHB, P-3	2/10/20 05:46		Within dropsonde circle	P-3 RF10, 7.5 km altitude Station 4
RHB, P-3	2/11/20			P-3 RF11, 7.5 km altitude

		10:26			Station 4
RHB, SD 1064	2/8/20 9:30	2/10/20 18:50	0.7 to 3.6	2/8/20 9:30 – 18:10 SD was 2.8 – 3.6 NM upwind, 2/8 19:00 0 2/10 18:50 SD was 0.7 – 0.8 NM from ship Station 4
RHB, BCO	1/24/20 18:20	1/25/20 23:40	20	RHB located directly upwind of BCO

A comparison of atmospheric and oceanic parameters measured onboard the ship and NTAS-18 was conducted Jan. 12 to 13. The comparison included a CTD (conductivity, temperature, and depth) sensor mounted on the ship's rosette and conductivity and temperature sensors attached to the NTAS mooring line. While waiting for the weather to calm down enough to recover NTAS-17, 6 SWIFTs were deployed. The ship transited 55 NM to the northwest and deployed the first SWIFT (22) on Jan. 14 at 01:13 UTC at 15° 41' 21" N, 51° 22' 5" W (Fig. 1, Table 2). Following a southeast track, the remaining 5 SWIFTs were deployed 5 to 12 NM apart across horizontal gradients in ocean surface current and temperature. SWIFT17, the second one deployed, was recovered due to the failure of a 3-D sonic anemometer. The ship returned to SWIFT17 to swap out the anemometer. It was re-deployed near its original position on Jan. 14 at 18:11 UTC. After each SWIFT deployment, underway CTD (uCTD) casts were performed to a depth of 50 m for comparison to SST and salinity measured onboard the SWIFTs and to understand the ocean mixed layer structure at the beginning of each SWIFT Lagrangian drift. In addition, the ship sat near each SWIFT for at least an hour after deployment for a comparison of measured near surface atmospheric and surface sea water parameters.

The ship returned to S1 and conducted a second comparison with NTAS-17 on Jan. 15 to 16, including a CTD cast with the ship's rosette and sensors on the NTAS mooring line. NTAS-17 was recovered on Jan. 16. The ship stayed at S1 and was within the P-3's dropsonde circle during its first flight (Research Flight 1 or RF1) on Jan. 17 from 15:30 to 16:40. A first comparison between the uCTD and the CTD on the ship's rosette for temperature and salinity was conducted on Jan. 17 at 22:36. The ship's CTD cast went to a depth of 500 m.

With the NTAS and MOVE work finished, the ship transited downwind on Jan. 18 for 14.5 hours to Station 2 (S2) located at 14º21'44"N and 53ºW (Fig. 1a). This location was downwind of the projected paths of the SWIFTs but still upwind of the EUREC[4]A study region. During the transit, aerosol and flux measurements were compromised by relative winds abaft the beam but surface ocean and meteorological measurements as well as radiosonde launches continued. In addition, uCTD casts to 100 m depth were made every hour to investigate a large-scale SST gradient between NTAS and S2. The ship briefly slowed to 2 to 4 kts for each cast.

The ship reached S2 on Jan. 19 at 01:30 UTC and turned into the wind for optimal aerosol and flux measurements. Underway CTDs were conducted to a depth of 100 m every 6 hr. The second overflight of the P-3 (RF2) occurred on Jan. 19 at 14:57 UTC with the *RV Ronald H. Brown* within the aircraft's dropsonde circle. A second comparison between the uCTD and the CTD on the ship's rosette was conducted on Jan. 21 at 16:15 with the ship's CTD reaching a depth of 150 m.

227   On Jan. 22 at 07:30 UTC, the ship left S2 to recover the SWIFTs before the end of Leg 1. The SWIFTs had drifted

228   between 53 and 103 NM to the southwest with those deployed at the more southern locations drifting the furthest

229   (Fig. 1a, Table 2). The ship transited 32 NM to the north to reach the southernmost SWIFT and then followed a

230   course to the northeast recovering the remaining SWIFTs which were 7 to 24 NM apart. Once all SWIFTs were

231   onboard (Jan. 22 19:14), the ship transited 180 NM to the southwest to 14° 22' 59"N and 55°W to be in the center of

232   the P-3's dropsonde circle the next day. Aerosol and flux measurements were compromised during the transit due to

233   the relative wind being abaft the beam.

234

235   The ship reached the designated position on Jan. 23 at 10:30, turned into the wind for optimal aerosol and flux

236   measurements, and was within the P-3's dropsonde circle on Jan. 23 at 14:06 (RF3). Later in the flight (15:42), the

237   P-3 flew over the ship at an altitude of 150 m. This flyby was the closest the P-3 was to the ship during the

238   ATOMIC campaign while all instrumentation was operational. At 22:00 the ship started the 250 NM transit back to

239   Bridgetown with a planned stop upwind of BCO/BACO for a measurement comparison. Initially, relative winds

240   were from the port side of the ship at -100° relative to the bow but 6 hrs into the transit they shifted to a relative

241   direction of -50° due to a change in true wind direction and the ship's course, making for better conditions for

242   aerosol and flux measurements. Radiosonde launches were halted on Jan. 24 at 2:45 near 56°W with the knowledge

243   that sondes launched from the *RV Meteor* and BCO could be used to fill in the gap. The ship arrived at the

244   comparison point 20 NM east of BCO (13° 8' 55.7"N, 59° 4' 59.2"W) at 18:20 on Jan. 24 and stayed until Jan. 25 at

245   23:40 (Fig. 1a). Underway CTDs were conducted approximately every 2 hours until Jan. 25 at 21:58.

246

247   The ship ended Leg 1 with a transit around the southern end of Barbados and into Bridgetown with an arrival on Jan.

248   26 at 12:15 for open house and outreach activities to be conducted on Jan. 27.

249

250   **2.2. Sampling events during Leg 2**

251

252   During Leg 2, the SWIFTs were deployed at the beginning of the leg and then recovered along with the

253   Wave Gliders at the end of the leg. Similar to Leg 1, measurements were made throughout the leg to

254   characterize atmospheric and oceanic conditions upwind of the EUREC[4]A study region.

255

256   The *RV Ronald H. Brown* left Bridgetown at 22:15 on Jan. 28 and headed for Station 3 (S3) located 290 NM to the

257   northeast of BCO/BACO at 13° 54' 0"N and 54° 30' 0"W (Fig. 1a). S3 was roughly halfway between BCO/BACO

258   and NTAS. Radiosonde launches began on Jan. 29 at 6:45 and continued every 4 hrs. The ship veered off its NE

259   track on Jan. 29 at 20:18 and turned to the southeast to map the spatial orientation of SST fronts with gradients

260   around 0.75°C for determining where to deploy SWIFTs. When done with mapping, the ship went north on Jan. 30

261   at 4:15 arriving in the vicinity of S3 and Wave Glider 245 at 08:00. Wave Glider 245 was recovered to replace

262   malfunctioning sensors.

263

Deleted: .

Formatted: Font: 11 pt

Formatted: Font: 11 pt

265   The ship zigzagged to the northwest and then northeast until reaching 14° 13' 25" N and 54° 43' 53" W on Jan. 30 at

266   17:12 where the first SWIFT deployment of Leg 2 took place (Fig. 1b, Table 2). The remaining SWIFTs were

267   deployed on a southeast track approximately 6 NM apart. After each SWIFT deployment, uCTD casts were

268   performed to a depth of 100 m to provide a subsurface context for SWIFT measurements. During each cast, the ship

269   moved into the wind at 0.5 kts. Wave Glider 245 was re-deployed on Jan. 30 at 18:08 after the last SWIFT was put

270   in the water. The ship then transited back to S3, arriving 5 hrs later at 23:09. During this 6 hr period, as the ship was

271   maneuvering to deploy SWIFTs, relative winds were from the port side between -50 to -100 degrees compromising

272   aerosol and flux measurements.

273

274   The ship remained at S3 until Feb. 3 at 15:00 to characterize diurnal variations in oceanic and atmospheric

275   conditions and to be in position for the P-3's RF5 and RF6. Continuous atmospheric and surface ocean

276   measurements were made, radiosondes were launched every 4 hrs, and uCTD casts were conducted every 2 hrs.

277   Four comparisons between the uCTD and the CTD on the ship's rosette were conducted between Feb. 1 and Feb. 3

278   with the ship's CTD reaching a depth of 400 m. The ship was at the center of the P-3's dropsonde circle on Jan. 31

279   at 16:25 (RF5) and Feb. 3 at 14:13 (RF6).

280

281   On Feb. 3 at 19:30 the ship headed back to Bridgetown for a medical emergency. Aerosol and flux measurements

282   were compromised due to relative winds abaft the beam. Radiosonde launches continued every 4 hours. The last

283   launch before reaching port was on Feb. 4 at 10:45. The ship arrived in Bridgetown on Feb. 4 at 19:00.

284

285   The ship departed Bridgetown on Feb. 6 at 16:00 and headed northeast to Station 4 (S4) located at 13º51'N and

286   54º51'36"W, 21.2 NM southwest of S3. Atmospheric measurements resumed along with radiosonde launches every

287   4 hrs. The ship arrived at S4 on Feb. 8 at 01:00 but left 6 hrs later to recover Wave Glider 245 because it was

288   experiencing navigation problems that could have endangered the vehicle. The Wave Glider was recovered 36 NM

289   to the northeast of S4 (14° 4' 55" N, 54° 17' 12" W) on Feb. 8 at 12:45. Aerosol and flux measurements were

290   compromised during the downwind transit back to S4 between 12:45 and 16:25. Once back on station, optimal

291   aerosol and flux measurements resumed along with uCTD casts every 2 hrs. A CTD cast to a depth of 1000 m with

292   the ship's rosette was conducted on Feb. 8 at 17:00 for comparison to the uCTD.

293

294   Still at S4, the ship was within the P-3's night time dropsonde circle on Feb. 9 (RF9) at 5:57. The NOAA PMEL-

295   operated Saildrone 1064 completed a first leg between BCO and NTAS and then sailed near the ship for a

296   comparison of fluxes and measured meteorological and seawater parameters. The Saildrone was 2.8 to 3.6 NM

297   upwind of the ship between Feb. 8 from 9:30 to 18:10 and within 0.7 to 0.8 NM of the ship between Feb. 8 19:00

298   and Feb. 10 18:50. Two final comparisons between the uCTD and the CTD on the ship's rosette were conducted on

299   Feb. 8 and Feb. 9 with the ship's CTD going to depths of 1000 and 400 m, respectively. The ship remained at S4 for

300   the P-3's second night flight (RF10) and was within the dropsonde circle on Feb. 10 from 05:46 to 06:42. The ship's

Deleted: making c

Deleted: launching

Deleted: conducting

304 final coordination with the P-3 occurred during a combination research and sightseeing flight with press (RF11) on
305 Feb. 11. The ship was not within the dropsonde circle but was flown over at sunrise at 10:26.
306
307 The ship remained at S4 until Feb. 10 at 12:00 at which point aerosol measurements were ended and the ship began
308 the transit to recover SWIFTs and Wave Glider 247. Recovery operations were conducted between Feb. 10 15:00
309 and Feb. 11 18:15. The four SWIFTs (16, 22, 23, and 24) that were initially deployed to the north between 14° 13'
310 25" and 13° 58' 39" N drifted to the northwest travelling a total distance ranging from 31 to 68 NM (Table 2, Fig.
311 1b). The two SWIFTs (17 and 25) deployed to the south between 13° 53' 40" N and 13° 48' 50" N initially drifted to
312 the southwest, each traveling 130 NM. The ship transited to the northeast to pick up the northern cluster of SWIFTs
313 first, staying near each asset for up to 1.5 hrs for a comparison of measured atmospheric and oceanic parameters.
314 The ship then did several back-and-forth tracks between the position of Wave Glider 247 and SWIFT 17 mapping a
315 SST front before recovering the Wave Glider and the last two SWIFTs.
316
317 After the SWIFTs and Wave Glider were recovered, the ship started a northeast transit on Feb. 11 around 19:30
318 across a SST front in the upwind direction to study air-sea interaction and atmospheric and oceanic mixed layer
319 variability. Underway CTDs were made continuously. On Feb. 12 at 06:00, the ship began the southwest transit back
320 to Bridgetown for the final time. Atmospheric sampling was compromised during the downwind transit. The last
321 radiosonde launch occurred on Feb. 12 at 10:45. The ship arrived in port on Feb. 13 at 10:00.
322
323 **2.3. NTAS operations and measurements**
324
325 NTAS was established to provide accurate air-sea flux estimates and upper ocean measurements in a region with
326 strong SST anomalies and the likelihood of significant local air-sea interaction on interannual to decadal timescales
327 (Weller, 2018;Bigorre and Galbraith, 2018). The station is maintained at a site near 15°N and 51°W through
328 successive mooring turnarounds. During Leg 1, the Upper Ocean Processes Group of the Woods Hole
329 Oceanographic Institution (WHOI) and crew of the *RV Ronald H. Brown* deployed the NTAS-18 mooring and
330 recovered the NTAS-17 mooring at nearby sites. Both moorings used Surlyn foam buoys as the surface element.
331 These buoys are outfitted with two Air–Sea Interaction Meteorology (ASIMET) systems (Colbo and Weller, 2009).
332 The ASIMET system measures, records, and transmits via Iridium satellites the surface meteorological variables
333 necessary to compute air–sea fluxes of heat, moisture and momentum. The upper 160 m of the mooring line are
334 outfitted with oceanographic sensors for the measurement of temperature, salinity and velocity. Information on the
335 instruments providing real-time data, measured atmospheric and oceanic parameters, and height/depth of the
336 measurements on the NTAS mooring are provided in Table 4.
337
338

340 **Table 4.** Instrumentation providing real-time data onboard the NTAS mooring.

Instrument	Measured/derived quantities, raw sampling interval	
	Atmospheric parameters	**Height (m)**
ASIMET system	Bulk air-sea fluxes, relative humidity, temperature, pressure, wind speed and direction, precipitation rate, longwave radiation, shortwave radiation, 1 min	3
	Oceanic parameters	**Depth (m)**
ASIMET system	Sea surface temperature and salinity, 1 min	0.8
Seabird (SBE-37 IM)	Temperature and salinity, 5min	10
NORTEK Aquadopp	Currents, 20 min	13
Seabird (SBE-37 IM)	Temperature and salinity, 5min	25
Seabird (SBE-37 IM)	Temperature and salinity, 5min	40
Seabird (SBE-37 IM)	Temperature and salinity, 5min	55
Seabird (SBE-37 IM)	Temperature and salinity, 5min	70

341

342

343 ASIMET data are sampled and recorded internally every minute. The oceanographic measurements are recorded

344 either every 5 min or 10 min for temperature and salinity (depending on the instrument type) and 20 min or 1 hr for

345 currents. The NTAS-18 mooring was deployed on Jan. 10 at 14° 44' N, 50° 56' W with anchor drop at 17:45 in

346 5055 m of water. The NTAS-17 mooring was recovered on Jan. 16 with anchor release at 10:41. Both buoys have a

347 watch circle of about 2 NM from their respective anchors and were separated by about 6 NM during the January 10

348 to 16 period allowing for comparisons of measured ocean and atmosphere parameters. Atmospheric data from

349 NTAS-17 and NTAS-18 were combined for comparison to measurements onboard the *RV Ronald H. Brown* (Sect.

350 4.2.1).Wind speed, air temperature, and specific humidity were adjusted to a height of 10 m and neutral atmospheric

351 stability using the COARE 3.6 bulk model for the comparison (Fairall et al., 2003;Edson et al., 2013). NTAS data in

352 the ATOMIC archive only include data collected during the ATOMIC campaign.

353

354 On Apr. 8, 2020 at 08:00 UTC, the NTAS-18 buoy went adrift. It meandered slowly toward the Caribbean for 7

355 months until being recovered on Oct. 20, 2020. NTAS-19 was deployed on Oct. 22, 2020.

356

357 **2.4. Shipboard atmospheric measurements**

358

359 Instrumentation onboard the *RV Ronald H. Brown* for the measurement of atmospheric and aerosol parameters is

360 listed in Table 5. Locations of instruments on deck are shown in Figure 3. NOAA's Physical Science Laboratory

361 (PSL) collected data to enable a deeper understanding and quantification of cloud processes, the environments in

362 which they either grow or dissipate, how the ocean and atmosphere interact, and the spatial variability of these

363 processes. Instrumentation mounted on the bow mast and forward O2 deck (two levels above the main deck)

364 measured sea-surface meteorological properties, rain rate, radiative fluxes, and air-sea turbulent fluxes using bulk,

365 eddy covariance, and inertial dissipation methods (Fairall et al., 1997;Fairall et al., 1996;Fairall et al., 2003;Edson et

366 al., 2013). Vertical profiles of backscatter from a ceilometer mounted on the forward O3 deck (three levels above the

367 main deck) provided cloud base height and temporal cloud fraction. For comparison with other platforms (NTAS

368 and Saildrone 1064), wind speed, air temperature, air pressure, and specific humidity were adjusted to a height of 10

369 m using the COARE 3.6 bulk algorithm. Final data products of meteorological and navigation data are 1-min and

370 10-min averages of high-resolution raw data (see Table 5 for raw sampling intervals). The data are time-stamped at

371 the beginning of the 1- and 10-min period. Fluxes were calculated at 10-min resolution, then interpolated to 1-min.

372

373 University of Miami (UM) provided high resolution measurements of cloud and rain to better understand the

374 relationship between cloud properties and cloud spatial organization as a function of cloud mesoscale organization,

375 in particular rain and the associated atmospheric cold pools (Stevens et al., 2020;Löffler-Mang and Joss, 2000). Two

376 collocated Parsivel disdrometers mounted on the forward O3 deck provided precipitation intensity, drop number,

377 and equivalent radar reflectivity. A sky camera provided a 50° field of view oriented horizontally off the starboard

378 side of the ship every 4 sec. A microwave radiometer was deployed to provide cloud liquid water path estimates but

379 its data acquisition was unsuccessful and no data are available A Marine Atmospheric Emitted Radiance

380 Interferometer (M-AERI) was mounted on the port side O2 deck rail (2 levels above the main deck) (Minnett et al.,

381 2001). It measured the spectra of infrared emission from the sea surface and atmosphere for the derivation of skin

382 **Table 5**. Instrumentation onboard the *RV Ronald H. Brown* for the measurement of atmospheric and aerosol
383 parameters. The O2 and O3 decks were two and three levels above the main deck, respectively. [a]Aerosol inlet was
384 located on the O2 deck, 18 m.a.s.l. Final data products of meteorological and navigation data are 1-min and 10-min
385 averages of high-resolution raw data and time-stamped at the beginning of the 1- and 10-min period. Fluxes were
386 calculated at 10-min resolution, then interpolated to 1-min for those files.
387

Instrument	Measured/derived quantities, raw sampling interval	Location
Atmospheric parameters		
Gill WindMaster Pro 3-axis ultrasonic anemometer	Wind vector, stress, and sensible heat flux, 0.1 sec	Bow mast
Optical precipitation sensor, OSI Inc., ORG-815 DA	Rain rate, 5 sec sampling, collected/recorded every 1 min	Bow mast
Li-COR 7500 Gas Analyzer	Water vapor density, turbulent latent heat flux, 0.1 sec	Bow mast
Vaisala HMT335	Air temperature, humidity, 1 min	Bow mast
Vaisala PTB220	Atmospheric pressure, 1 min	O2 deck
2 Eppley PSPs (Pyranometer)	Shortwave radiation, 1 min	O2 deck
2 Eppley PIRs (Pyrgeometer)	Longwave radiation, 1 min	O2 deck
Systron and Donner MP-1 6-axis motion detector system	3-D ship acceleration, 0.1 sec	Bow mast
Vaisala CL31 Ceilometer	Vertical profiles of backscatter from refractive index gradients, cloud base height, cloud fraction, 15 sec sampling from 0-7.7 km with 10 m vertical spacing	O3 deck
2 Parsivel optical rain gauges, 650 and 780 nm	Rain rate, equivalent radar reflectivity, particle number	O3 deck
StarDot Camera, NetCam XL	Pointed to starboard, field of view of 50°, image captured every 4 sec	O3 deck
Doppler lidar λ=1.5 μm	Atmospheric vertical velocity and backscatter intensity, horizontal wind profiles, estimates of cloud base and mixed layer heights; 0.5 sec	O2 deck
W-band (95.56 GHz) Doppler vertically pointing cloud radar	Vertical profiles of non-precipitating and lightly-precipitating clouds from 100 m to 4.2 km with 30 m vertical resolution every 0.5 sec	O2 deck
Dual-flow, two filtered radon detector	^{222}Rn, 30 min	O3 deck
Vaisala WXT536	T, RH, rain rate; 1 sec	O2 deck
Picarro water vapor isotope analyzer (L2130-fi)	Water vapor concentration and isotopic composition, 0.2 sec	Aerosol inlet[a]
Vaisala RS-41 radiosondes	Profiles of T, RH, P, and winds every 4 hrs	Main deck
Thermo Environmental Model 49C	Ozone, 1 sec	Inlet at 18 m.a.s.l.
Aerosol Properties		
Collection with multi-jet cascade impactors and analysis by ion chromatography, thermal-optical, gravimetric, and XRF analysis	Size segregated concentrations of Cl$^-$, NO$_3^-$, SO$_4^{2-}$, methanesulfonate (MSA$^-$), Na$^+$, NH$_4^+$, K$^+$, Mg^{+2}, Ca^{+2}, organic carbon, elemental carbon, trace elements; hours	Aerosol inlet[a]
DMPS and TSI 3321APS	Number size distribution 0.02 to 10 μm, 5 min	Aerosol inlet[a]

TSI 3025A, 3760A, 3010	Number concentration > 3, 13, 13 nm; 1 sec	Aerosol inlet[a]
TSI 3563 Nephelometer	Sub-1.1 and sub-10 μm light scattering and backscattering; 450, 550, 700 nm; 60% RH; 1 sec	Aerosol inlet[a]
TSI 3563 Nephelometers	Sub-1.1 μm scattering f(RH); 450, 550, 700 nm; dry and 80%RH; 1 sec	Aerosol inlet[a]
Radiance Research PSAP	Sub-1.1 and sub-10 μm light absorption; 467, 530, 660 nm; dry	Aerosol inlet[a]
DMT CCNC	Sub-1.1 μm cloud condensation nuclei concentration, 0.1 to 0.6% S, 1 sec	Aerosol inlet[a]
Solar Light Microtops Sunphotometer	Aerosol Optical Depth; 380, 440, 500, 675, 870 nm	O3 deck

388
389
390
391
392
393
394
395

Figure 3. Instrumentation onboard the *RV Ronald. H. Brown* for the measurement of atmospheric and oceanic parameters located on a) the bow mast and forward O2 deck and b) port side O3 deck. Asset deployments are shown for c) NTAS mooring, d) ship's rosette with CTD and Niskin bottles, e) uCTD, f) SWIFT, g) Wave Glider, and h) radiosonde. Also shown are i) P-3 fly over of the ship on Jan. 23 and j) Saildrone upon its return to the U.S. (Newport, RI) from Barbados. Not shown are disdrometers on the port O3 deck and camera on the starboard O3 deck.
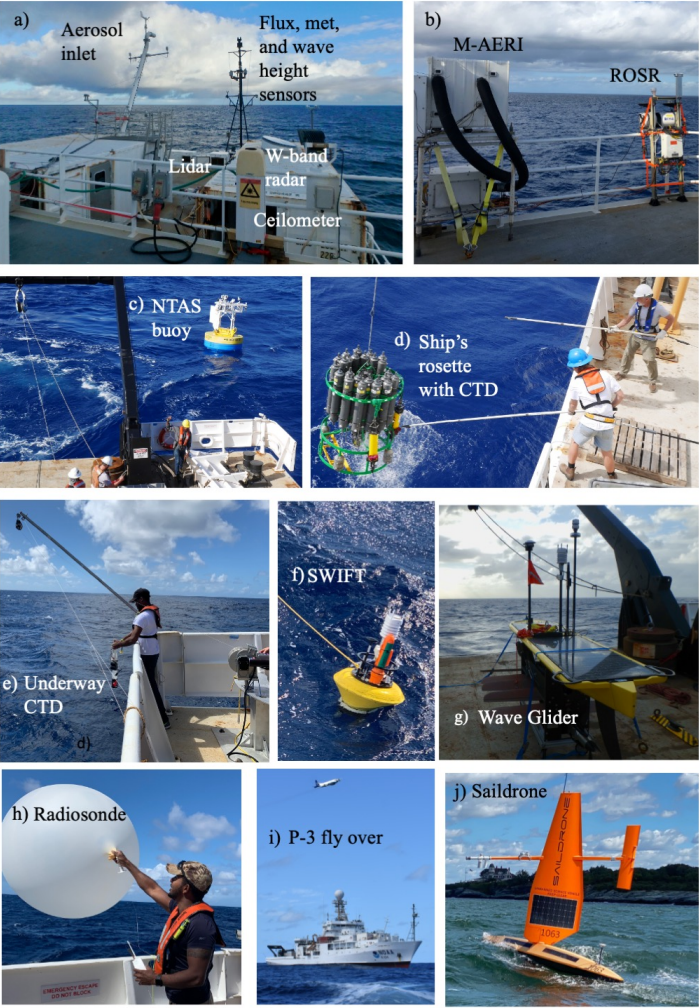
403 sea surface temperature and lower troposphere profiles of temperature and humidity (Szczodrak et al., 2007). A W-

404 band Doppler vertically pointing cloud radar was housed in a container on the O2 deck for the measurement of

405 vertical profiles of non-precipitating and lightly-precipitating clouds (Moran et al., 2012). The radar was not

406 functional during Leg 1 and operated with a 10 dB attenuator on Leg 2 that prevented detection of non-precipitating

407 clouds. Although the loss of this information limited the ship-based observations of non-precipitating clouds, data

408 from the shipboard ceilometer and Doppler radar and the cloud radar on the P-3 will be used to fill in gaps.

409

410 NOAA's Chemical Sciences Laboratory (CSL) operated a microjoule class, pulsed Doppler lidar (microDop)

411 operating at a wavelength of 1.5 μm to assess atmospheric turbulence, aerosol backscatter intensity, and horizontal

412 winds (Schroeder et al., 2020). The lidar was mounted on the forward O2 deck. The system was motion stabilized

413 while staring vertically to within 0.25 degrees of zenith. Ship motion projected onto the line-of-site velocity

414 measurement was estimated and removed using a 6-axis inertial navigation unit (INU). The INU allowed the lidar to

415 measure the mean and turbulent motions of aerosol in clear air and cloud scatterers with a spatial and temporal

416 resolution of 33.6m and 2Hz respectively. The first valid gate was 75m above the ocean surface. The maximum

417 height of valid data depends on the availability of aerosol scattering targets. Typically, the instrument provided data

418 through the top of the marine atmospheric boundary layer, in the presence of elevated dust layers to 3km, and clouds

419 to a height of 7km. The lidar pointed vertically 95% of the time to sample updrafts and downdrafts in the subcloud

420 mixed layer and in the interstitial trade cumulus boundary layer and spent 2 minutes of every hour performing a 65°

421 elevation, full azimuthal scan to measure horizontal wind profiles. Real-time quicklooks of backscatter intensity

422 profiles showing strongly scattering cloud base and updraft structures were available for awareness of the clouds and

423 turbulent mixed layer throughout the cruise. Cloud base height (CBH) was retrieved by applying Haar wavelet

424 covariance transforms to the backscatter intensity profiles.

425

426 Oregon State University and the National Center for Atmospheric Research (NCAR) operated a Picarro water vapor

427 isotope analyzer on Leg 2 of the cruise to investigate processes that shape the atmosphere's humidity structure and

428 its variations. The spectroscopic analyzer measured water vapor concentration and its isotopic composition, the

429 isotope ratios of oxygen ($^{18}O/^{16}O$) and hydrogen (D/H). All three quantities were measured continuously at 5 Hz

430 frequency via the aerosol inlet on the O2 deck at 18 m above sea level (m.a.s.l.). Complementary gas-phase water

431 isotopic measurements were made from the P-3, at BCO, from the French ATR aircraft, and aboard German and

432 French research vessels. Rainwater and seawater were also collected from the ship platforms for future offline

433 analysis. Surface sea water and water column samples from CTD casts were also collected to investigate the upper

434 ocean mixing and the freshwater balance to be evaluated in the context of air-sea gas exchange and upper ocean

435 circulation.

436

437 The goals of NOAA's Pacific Marine Environmental Laboratory (PMEL) were to assess the impacts of aerosols on

438 clouds and direct aerosol light scattering and absorption on the temporal variability of net radiation reaching the

439 ocean surface and SST for the conditions of a well-mixed boundary layer. Measurements included aerosol chemical

Formatted: Pattern: Clear (White)

Formatted: Font: (Default) Times New Roman, 10 pt

Deleted: impact of aerosol-cloud interactions

441 composition, total number concentration, number size distribution, light scattering and its dependence on relative
442 humidity, light absorption, and cloud nucleating ability. Aerosol instrumentation was housed in two containers on
443 the O2 deck. All instruments drew sample air from an inlet 18 m.a.s.l. mounted on top of one of the O2 deck vans
444 (Bates et al., 2002) (Fig. 3). Aerosol optical depth (AOD) was measured using Microtops hand held sunphotometers.
445 The raw Microtops data were processed by the NASA Maritime Aerosol Network in conjunction with the Aerosol
446 Robotic Network (Smirnov et al., 2009). In addition, ^{222}Rn was measured for its use as a tracer of continentally-
447 influenced air masses (Whittlestone and Zahorowski, 1998) and O_3 was measured for its use as an indicator of
448 entrainment from the upper troposphere.
449
450 Radiosondes were launched throughout the ATOMIC campaign to provide information about the temporal evolution
451 and vertical structure of the boundary layer, upper atmosphere, and clouds. A total of 97 radiosondes (Vaisala RS41-
452 SGP) were launched from the fantail during Leg 1 and 66 were launched during Leg 2. There were 6 launches per
453 day at 02:45, 06:45, 10:45, 14:45, 18:45, and 22:45 UTC. Vertical profiles of pressure, temperature, relative
454 humidity, and winds were measured from the surface to approximately 25 km. Measurements were also made during
455 the radiosondes' descent. Data were communicated to the Global Telecommunications System (GTS) following
456 each sounding via email to the U.S. National Weather Service and via FTP to MeteoFrance. The data were put into
457 10 m altitude bins and merged with the EUREC^{4}A sounding network. Raw (Level-0), quality-controlled 1-second
458 (Level-1), and vertically gridded (Level-2) data in NetCDF format are available to the public at AERIS
459 (https://doi.org/10.25326/62). The methods of data collection and post-processing can be found in (Stephan et al.,
460 2020).
461
462 Radiosonde operations were suspended on the ship west of ~56°W when the ship transited to Bridgetown for the
463 planned in port (Jan. 24 at 2:45) and an emergency medical evacuation (Feb. 4 at 10:45). Soundings from BCO were
464 stitched together with those from the ship to allow for an uninterrupted data record over the entire cruise.
465
466 The Lifted Condensation Level (LCL) was calculated from the BCO-RHB radiosonde data record and assumed to
467 represent Cloud Base Height (CBH). The LCL (in m) was calculated as
468
469 $\qquad$ LCL = $(T_{50} - T_{d,50})$ x 125 + 50 $\qquad\qquad\qquad\qquad$ (1)
470
471 where T_{50} is temperature and $T_{d,50}$ is dew point, both at 50 m height (Espy, 1836;Bolton, 1980). The lowest altitude
472 considered was 50 m to avoid contamination by the temperature and relative humidity near the ship's deck and to
473 minimize the effect of vertical gradients in the surface layer. Since the calculation started at 50m, 50 was added to
474 the LCL.
475
476 **2.5. Shipboard oceanic measurements**
477

480   Instrumentation onboard the *RV Ronald H. Brown* for the measurement of oceanic parameters is listed in Table 6.

481   Locations of instruments mounted on the deck are shown in Figure 3. As stated above, UM's M-AERI, located on

482   the port side forward O2 deck, measured sea surface skin temperature (Minnett et al., 2001).

483   **Table 6**. Instrumentation onboard the *RV Ronald H. Brown* for the measurement of seawater parameters. O2 deck is
484   two levels above the main deck.

485

Instrument	Measured /derived quantities, raw sampling interval	Location
Marine Atmospheric Emitted Radiance Interferometer (M-AERI)	Sea surface skin temperature, 5 – 7 min averages	O2 deck
Remote Ocean Surface Radiometer (ROSR)	Sea surface skin temperature, 5 min averages	O2 deck
Floating YSI 46040 Thermistor (Sea snake)	Sub-skin sea surface temperature, ~ 0.05 m depth, 1 sec	Deployed off port side with outrigger
Riegl 1-D laser altimeter	Wave height and period, 10 min averages	Bow mast
Seabird 9+ CTD	At station conductivity (salinity), temperature, depth (pressure), PAR, fluorescence, and oxygen	Deployed off starboard side, main deck
Seabird SBE45 thermosalinigraph Seabird SBE38 thermistor	Seawater temperature, conductivity (salinity), 1 sec	5.3 m below the surface
Acoustic Doppler Current Profiler 75 kHz (ADCP)	Current velocity across 2 depth ranges depending on mode. Narrowband: 29-892 m. Broadband: 17-333 m. 5 min sampling.	Ship's hull
RBR Concerto underway CTD + Tuna Brute winch (uCTD)	Conductivity (salinity), temperature, and depth (pressure) from the surface to 60 or 130 m depending on cast	Deployed off starboard aft quarter

486

487   During Leg 1, the Applied Physics Laboratory at the University of Washington (APL-UW) also measured sea

488   surface skin temperature with a Remote Ocean Surface Radiometer (ROSR) located near the M-AERI. PSL

489   measured sub-skin temperature at approximately 0.05 m depth with a floating thermistor (a.k.a sea snake) deployed

490   off the port side. A skin temperature value was estimated by the COARE algorithm using the sea snake data as input

491   (Fairall et al., 1996;Fairall et al., 1997). This algorithm accounts for the cool skin present in the upper ~0.2-1 mm

492   and any potential diurnal warm layers in the upper ~10 m. This COARE-calculated skin T and the current-relative

493   wind were used to compute bulk, eddy covariance, and inertial dissipation air-sea fluxes (Fairall et al., 1997;Fairall

494   et al., 2003). The COARE 3.6 algorithm estimated wave parameters using wind as input. The parameterization is

495   based on fits to the Banner and Morison (2010) wave model and the flux database collected by NOAA PSL,

496   University of Connecticut, and Woods Hole Oceanographic Institution (Fairall et al., 2003;Edson et al., 2013). PSL

497   also measured significant wave height and period with a 1-dimensional downward looking RIEGL laser altimeter

498   mounted on the bow mast.

499

500   The ship's rosette-mounted CTD was intermittently deployed off the starboard main deck for comparison to the

501   uCTD, Wave Gliders, SWIFTs, and NTAS moorings. Water was collected from the Niskin bottles for analysis of the

502   isotopic composition of oxygen and hydrogen. In addition, the ship had an underway seawater sampling system

503   consisting of a thermistor SBE38 located at the intake valve on the hull and a thermosalinograph SBE45 located

504   inside the ship. These sensors produced underway measurements of temperature and conductivity (salinity) from

505   water sampled at ~5.3 m below the surface. The values recorded may be representative of seawater properties

506   shallower in depth due to an unknown amount of mixing along the hull of the ship that is dependent on currents,

507   ship speed, and waves. The ship also had a 75 kHz acoustic Doppler current profiler (ADCP) for the measurement of

508   currents at depths greater than ~ 17 m.

509

510 UW deployed an underway CTD (uCTD) for the measurement of conductivity (salinity), temperature, and pressure

511 (depth) to assess variability in the upper 60 to 130 m of the water column (Mojica and Gaube, 2020). The uCTD was

512 deployed off the starboard aft quarter. Initially, the probe was lowered by hand with line pre-measured to 50 m.

513 Casts were completed more frequently and with an electric winch after the NTAS mooring work was done which

514 freed up deck space. During Leg 2, a cast with the ship's CTD was conducted every day at 13:00 (Jan. 31, Feb. 1

515 and 2) or 17:00 (Feb. 3, 8, and 9) shortly after a uCTD cast. These casts were used to correct the uCTD conductivity

516 data which had a small offset due to interference from the sensor guard. A transect of intensive uCTD data was

517 collected when the ship transited from NTAS (S1) to S2 on Jan. 18. While at S2, uCTD casts were conducted every

518 1 to 4 hrs. In addition, uCTD casts were conducted every 2 hrs during the majority of Leg 2 when the ship was

519 stationary. The frequency of uCTD sampling increased to every 10 min between 13:00 and 15:15 on Feb. 9 to study

520 heaving of periodic internal waves located at the base of the mixed layer (60-80 m depth) and for 7 hrs at the end of

521 Leg 2 on Feb. 11 and 12 as the ship transited across a strong SST front in the upwind direction. uCTD casts were

522 also performed when deploying or recovering the SWIFTs and Wave Gliders for comparison purposes.

523

524 **2.6. Wave Glider measurements**

525

526 Two Wave Gliders (serial numbers 245 and 247) operated by APL-UW were deployed within 15 minutes of each

527 other on Jan. 9 (Fig. 1a and Table 2). The Wave Gliders greatly increased the sampling of spatial inhomogeneities in

528 atmospheric and oceanic properties as well as bulk air-sea fluxes in the study area (Thomson and Girton,

529 2017;Thomson et al., 2018). The deployment occurred on the transit to NTAS approximately 45 NM to the

530 southwest of the buoy with the intent of leaving the Wave Gliders in the water throughout the length of the cruise.

531 They were remotely piloted from shore via an online portal to cross gradients in SST and ocean currents. Data were

532 available in near real time which helped guide their course. The Wave Gliders were equipped with surface

533 meteorological sensors (bulk winds, air temperature, relative humidity, pressure, and longwave and shortwave

534 radiation), sky cameras, wave motion sensors, downward looking ADCPs for currents, and CTDs at 1 and 8 m depth

535 for conductivity (salinity) and temperature measurements at 1 and 8 m depth. Measurements were collected during

536 20-min bursts every 30 min. Final data products are 60-min averages of high-resolution raw data within each hour,

537 time-stamped at the beginning of the hour. Instrumentation onboard the Wave Gliders is listed in Table 7.

538

539 Wave Glider 245 was recovered, repaired, and redeployed on Jan 30. Telemetered data suggested that the humidity

540 sensor had malfunctioned. When recovered, it was found that the radiometers and their entire mounting pole were

541 gone, water was inside the data logger housing, the Airmar meteorological sensor and light were broken, and the

542 Vaisala meteorological sensor was destroyed. The radiation measurements lasted approximately one week into the

543 deployment. The Wave Glider was redeployed with spare Vaisala and Airmar meteorological sensors but no

544 radiometer. Wave Glider 245 was recovered for the final time on Feb. 7 because it was experiencing navigation

545 problems that could have endangered the vehicle. Wave Glider 247 sampled from Jan. 9 to Feb. 11. On Jan. 31,

546   Wave Glider 247 was inspected with the ship at close range after finding Wave Glider 245 damaged the day before.

547   The meteorological sensors were found to be in good condition but the radiometers had detached and were being

548   dragged by wires on the port side of vehicle. A small boat was deployed to clip the radiometer wires and take the

549   instruments back to the ship.

550

551   **Table 7**. Instrumentation onboard the Wave Gliders for the measurement of atmospheric and seawater parameters.
552   Data were collected during bursts lasting 20 min at the top of each hour. Measurements were collected during 20-
553   min bursts every 30 min. Final data products are 60-min averages of high-resolution raw data within each hour and
554   time-stamped at the beginning of the hour.

Instrument	Measured quantity	Height (+) Depth (-) (m)	Raw sampling interval
Airmar 200WX	Wind velocity (true and relative), GPS position, COG, SOG, magnetic heading, temp, pressure, pitch and roll	+1.3	1 sec
Vaisala WXT530	Wind velocity, air temperature, pressure, relative humidity, rain rate	+1	1 sec
Kipp Zonen CMP3 pyranometer	Short wave radiation (300-2800 nm)	+1	5 sec
Kipp Zonen CGR3 pyrgeometer	Long wave radiation (4200-4500 nm), temperature of sensor	+1	5 sec
GPSWaves/Microstrain 3DM-GX3-35 GPS/AHRS	Directional (2D) wave spectra, and standard bulk wave parameters of height, period, direction	0	0.25 sec
Aanderaa 4319	Conductivity, temperature	-0.24	2 sec
RDI Workhorse Monitor 300kHz ADCP	Ocean current profiles with 4 m vertical resolution	data between -6 to -100 m	1 second pings, ensemble averages recorded every 2 min
Seabird GPCTD+DO	Conductivity, temperature, depth, dissolved O2	-8 m	10 sec

555

556

557   **2.7. SWIFT measurements**

558

559   Drifting with ocean currents and winds, the SWIFTs (Surface Wave Instrument Floats with Tracking) offered a

560   Lagrangian view of the near-surface ocean and atmospheric properties, ocean waves and currents, bulk air-sea

561   fluxes, and cloud features (Thomson, 2012;Thomson et al., 2019). Instrumentation onboard SWIFTs v4 and v3 is

562   listed in Tables 8 and 9, respectively. Six SWIFT drifters were deployed in two SE-NW lines across gradients in

563   SST and ocean surface currents – once during Leg 1 and once during Leg 2. These gradients were identified with

564   satellite MUR v4 SST daily plots and the ship's underway thermistor, thermosalinograph, and ADCP. Two version 3

565   (serial number 16 and 17) and four version 4 (serial number 22, 23, 24, and 25) SWIFTs were deployed. All had

566   bulk meteorological sensors (winds, air temperature and pressure on all models, plus relative humidity on the v4

567   models), sky cameras, and CTD sensors at 0.3 m depth for measuring temperature and conductivity (salinity). The

568   v3 models also had conductivity and temperature sensors at 1.1 m depth. The v3 SWIFTs measured ocean

569   turbulence in the upper 0.62 m. The v4 SWIFTs measured ocean turbulence in the upper 2.64 m. Both versions had

570   ADCPs that measured vertical profiles of currents down to 20 m. The SWIFTs sampled high resolution bursts of

571 data for 8 min at the top of each hour. These data were archived on board the vehicle for final processing once

572 recovered. The 8-min data segments and platform location were also averaged and reported via Iridium satellite

573 telemetry each hour for monitoring purposes. SWIFT locations were also tracked in real time using the AIS ship

574 traffic system (local VHF radio signals). The SWIFTs were deployed for 8 days during Leg 1 (Jan. 14 to 22) and 13

575 days during Leg 2 (Jan. 30 to Feb. 11).

576

577 **Table 8**. Instrumentation onboard the version 4 SWIFTs (serial numbers 22, 23, 24, 25) for the measurement of
578 atmospheric and seawater parameters. Measurements were collected during 8-min bursts at the beginning of each
579 hour. Final data products are 8-min averages of high-resolution raw data, time-stamped at the beginning of each
580 hour.

Instrument	Measured quantity	Height (+) Depth (-) (m)	Raw sampling interval
Vaisala WXT530	Wind velocity, air T, barometric pressure, relative humidity, rain rate	0.5	1 sec
Camera	320 x 240 JPEG cloud images	0.2	4 sec
SBG Ellipse GPS/AHRS	Directional (2D) wave spectra, and standard bulk wave parameters of height, period, direction	0	0.2 sec
Nortek Signature 1000 ADCP with AHRS		-0.3 to -2.64	0.25 sec
	Turbulent kinetic energy dissipation rate profiles with 0.04 m vertical resolution		
	Ocean current profiles with 0.5 m vertical resolution	-0.35 to -20	0.25 sec
	3-D motion and heading data	0	0.25 sec
Aanderaa 4319	Conductivity (salinity), temperature	-0.3	2 sec

581
582

583 **Table 9**. Instrumentation onboard the version 3 SWIFTs (serial numbers 16 and 17) for the measurement of
584 atmospheric and seawater parameters. Measurements were collected during 8-min bursts at the beginning of each
585 hour. Final data products are 8-min averages of high-resolution raw data and time-stamped at the beginning of the
586 hour.

Instrument	Measured quantity	Height (+) Depth (-) (m)	Raw sampling interval
Airmar 200WX	Wind velocity, GPS position, COG, SOG, magnetic heading, air temperature and pressure, pitch and roll	0.8	1 sec
Camera	320 x 240 JPEG cloud images	0.2	4 sec
GPSWaves/Microstrain 3DM-GX3-35 GPS/AHRS	Directional (2D) wave spectra, standard bulk wave parameters of height, period, direction	0	0.25 sec
Nortek Aquadopp ADCP	Turbulent kinetic energy dissipation rate profiles with 0.04 m vertical resolution	-0.02 to -0.62	0.25 sec
	Ocean current profiles with 0.5 m vertical resolution	-0.65 to -20	0.25 sec
Aanderaa 4319	Conductivity (salinity), temperature	-0.50	2 sec
Aanderaa 4319	Conductivity (salinity), temperature	-1	2 sec

587
588

589 **2.8. Saildrone measurements**
590
591 NOAA sponsored two Saildrones for the ATOMIC campaign to obtain high quality multiscale air-sea fluxes (Zhang
592 et al., 2019) in two different regimes. Both were launched from Bridgetown, Barbados on Jan. 12, 2020. Saildrone
593 SD1063 focused on the large ocean eddies southeast of BCO, where the North Brazil Current Rings propagate
594 northwestward toward Barbados. Saildrone 1064 sampled in Trade Wind Alley along the leg between BCO and
595 NTAS. In addition, Saildrone 1064 coordinated sampling with the *RV Ronald H. Brown*, remote sensing from
596 research aircrafts, NTAS, Wave Gliders, and SWIFTs. Saildrones 1063 and 1064 were equipped to measure near
597 surface ocean temperature and salinity, upper-ocean current profiles (6m-100m), surface air temperature, humidity,
598 pressure, wind direction and speed, wave height and period, short- and long-wave radiation, and cloud images
599 (Table 10). This system enabled calculation of the bulk latent heat flux and direct turbulent fluxes of momentum and
600 sensible heat. Six thermistors were strapped on the keel to measure the surface layer stratification. Onboard data
601 processing included averaging and motion correction. One-minute averages (5-minute average for ADCP current)
602 were telemetered in real time, while high resolution data were downloaded after the Saildrones returned to U.S.
603 During the 1-month ATOMIC intensive observation period of Jan. 12 to Feb. 12, Saildrone 1064 continuously
604 measured air-sea interaction processes between BCO and NTAS and sailed 1777 nautical miles. After ATOMIC, the
605 Saildrones continued their observations until July 16 and then sailed back to the U.S. arriving in Newport, RI on
606 August 30, 2020.
607
608 Three additional Saildrones were piloted by a NASA-funded effort. These data and their details are posted at
609 https://podaac.jpl.nasa.gov/dataset/SAILDRONE_ATOMIC, https://doi.org/10.5067/SDRON-ATOM0.
610
611 **2.9. RAAVEN UAS measurements**
612
613 The University of Colorado operated a small remotely-piloted aircraft system (RAAVEN) from Morgan Lewis
614 Beach on the northeastern shore of Barbados between Jan. 24 and Feb. 16. The miniFlux payload flew onboard the
615 RAAVEN UAS (de Boer et al., 2020). Flights conducted during this campaign targeted the thermodynamic and
616 kinematic structure of the lower atmosphere, with sampling occurring between the surface and 1 km altitude. The
617 vast majority of the flights were focused on the sub-cloud layer, with extended sampling conducted at cloud base
618 and a sequence of set altitudes within the sub-cloud layer. Included in these flights were regular sampling intervals
619 at 20 m above the ocean surface to collect information on turbulent surface fluxes of heat and momentum. Most
620 flights were conducted in the near-coastal zone between 0 and 2 km from the coastline. MiniFlux sensors included a
621 multihole pressure probe (MHP); fine-wire array; IR thermometers; pressure, temperature and humidity sensors
622 similar to those used in radiosondes and dropsondes; redundant pressure, temperature, and humidity probes; and an
623 inertial navigation system.
624

625 **Table 10**. Instrumentation onboard the NOAA sponsored Saildrones. 1-minute averages (5-minute average for
626 ADCP current) were telemetered in real time except where noted below. Final data products are 1-min averages of
627 high resolution raw data.

Instrument	Measured quantity	Height (+) Depth (-) (m)	Raw sampling interval
Gill WindMaster 1590-PK	Wind velocity (true and relative), GPS position, COG, SOG, magnetic heading, temp, pressure, pitch and roll	+5.2	0.1 sec
Rotronic Hygroclip 2	Air temperature, relative humidity	+2.3	1 sec
SPN1 Delta-T Sunshine pyranometer	Short wave radiation	+2.8	0.2 sec
Eppley Precision Infrared Radiometer (PIR)	Long wave radiation, temperature	+0.8	1 sec
VectorNav VN300 DualGPS aided IMU (Wing)	GPS position, COG, SOG, magnetic heading, pitch and roll (motion correction for WindMaster and SPN1)	+2.575	0.05 sec
VectorNav VN300 DualGPS aided IMU (Hull)	Wave height and wave period and motion correction for ADCP currents	+0.34	0.05 sec
LICOR LI-192SA	Photosynthetically Active Radiation (PAR)	+2.6	1 sec
WET Labs ECO-Fluorometer	Chlorophyll-a (experimental)	-0.5	1 sec
RBR C.T.ODO.chl-a	Conductivity, temperature, dissolved O2, Chl-a (experimental)	-0.53	Inductive CTD
Teledyne RDI Workhorse 300kHz ADCP	Ocean current profiles	-6 to -100	1 sec, 5 min avg. sent via telemetry
Heitronics CT15.10	Skin seawater temperature (experimental)	0	1 sec
Vaisala PTB 210	Barometric pressure	+0.2	1 sec
4 Cameras	Cloud image	Upward, sideways, downward	Every 5 min, telemetered every 30 min
Seabird SBE57 temperature loggers	Temperature	-0.3, -0.6, - 0.9, -1.2, -1.4, -1.7	1 sec, 1 min avg. not telemetered
Seabird SBE37 CTD+DO	Conductivity, temperature, depth, dissolved O2	-0.5	Pumped, burst sampled 10 sec for 1min/5 min

628
629

630 **2.10. SVPS drifter measurements**

631

632 Though not deployed from the *R/V Ronald H. Brown*, the ATOMIC field campaign and its archive also includes a
633 dataset of 9 SVPS type surface ocean drifters deployed by NOAA AOML (Surface Velocity Program Salinity,
634 (Centurioni et al., 2015;Hormann et al., 2015)). These were deployed from the EUREC[4]A ship *RV L'Atalante* 50 to
635 150 NM from the South American coast, between 6ºN and 10ºN, the so-called Boulevard de Tourbillons (Eddy
636 Boulevard), where North Brazil Current Rings translate northwestward (Fig. 1b). The purpose of these drifters was
637 to measure air-sea interaction, ocean properties, and atmospheric variability amidst ocean eddies and low-salinity
638 plumes from a Lagrangian perspective. During ATOMIC the SVPS drifters measured air pressure and relative wind

639 at 0.5 m height. They also measured ocean salinity and temperature (0.3, 5, 10 m depth, with a duplicate T sensor at

640 0.3 m), and ocean velocity representative of water located between 11-19 m depth and centered at 15 m. The drifter

641 was equipped with a drogue centered at 15 m in the form of a long vertically-oriented holey sock. The drogue's full

642 extent spanned a depth of 11.34 m to 18.66 m. Therefore, currents calculated from the drifter location are

643 representative of currents between these depths. Bulk wind stress and the bulk drag coefficient were estimated from

644 these data using COARE 3.6. Data records began at different times and locations to sample different ocean features.

645 Four drifters started on Jan. 23, 1 drifter on Jan. 26, 4 drifters on Feb. 2, and 1 drifter on Feb 4. The drifters exited

646 the ATOMIC/EUREC4A region on about Apr. 29, which marks the end of this archived ATOMIC dataset. After

647 this date, data were still being reported from some sensors and can be accessed by contacting the PI (Table 11). The

648 drifter sensors sampled every 90 sec and then computed averages over 30 min. The averaged data were transmitted

649 to land via satellite telemetry. The position and time data were instantaneous every 30 min. Ten total drifters were

650 deployed but GPS did not work on one so that dataset is not posted.

651

652 **2.11. BACO aerosol measurements**

653

654 Size resolved cloud condensation nuclei (CCN) number concentrations were measured with a custom-made

655 differential mobility analyzer (DMA) for size selection connected to a Droplet Measurement Technologies (DMT)

656 CCNC-100 and a GRIMM 5.412 CPC. Aerosol number size distributions were made with a Scanning Mobility

657 Particle Sizer (SMPS) (GRIMM 5.420) with a diameter range of 0.10 to 1.094 μm. Measurements were made from

658 an isokinetic aerosol inlet located at roughly 47 m.a.s.l.

659

660 **2.12. BCO measurements**

661

662 BCO is at a height of 25 m.a.s.l. Meteorological sensors (Vaisala WXT-520) were mounted at 4 m.a.g.l. BCO

663 launched 182 radiosondes. Data from the sondes were merged into the EUREC[4]A sounding network (Stephan et al.,

664 2020). A Lufft ceilometer CHN 15k NIMBUS was used for the determination of cloud base height.

665

666 **3. Overview of meteorological and surface seawater conditions sampled**

667

668 During ATOMIC, the *RV Ronald H. Brown* primarily operated in Trade Wind Alley, north of 12.5°N between

669 ~56°W and NTAS (Fig. 1a). During the boreal winter, near-surface winds from the northeast carry air masses from

670 NTAS to BCO in about 1.5 d. Positioning the *RV Ronald H. Brown* in Trade Wind Alley allowed for sampling of

671 atmosphere and ocean conditions from the surface in between NTAS and BCO. Winds were fairly steady throughout

672 the cruise with an average speed (10 m) of 8.3 ± 2.1 m sec^{-1} and direction of $70 \pm 21°$ (Fig. 4a). Air temperature (10

673 m) ranged between 22.7 and 27.9°C and averaged 25.7 ± 0.61 °C. RH averaged $71 \pm 4.7\%$ (Figure 4b). Radiosondes

674 launched within Trade Wind Alley revealed dryer conditions in the lower and middle troposphere compared to

675 observations made to the south in the Boulevard de Tourbillons which paralleled the coast of South America (Fig.

676 1b). Stephan et al. (2020) attribute the difference to more frequent periods of a deep moist layer and deeper

677 convection to the south.

678

679 Rain rate was measured by three instruments during the cruise located at different places on the ship. Two Parsivel

680 disdrometers were located on the port rail on the O3 deck, an ORG-815 DA optical range gauge was located on the

681 mast tower, and a Vaisala WXT536 was mounted on top of an aerosol sampling van on the O2 deck. Although

682 instruments and locations were not identical, a coherent picture of rain occurrence emerges with frequent events

683 **Figure 4.** Time series of bow mast measurements of a) wind speed and direction, b) air temperature and relative
684 humidity all adjusted to 10 m height using the COARE 3.6 bulk model. Also shown are c) rain rate measured with
685 three different instruments, d) dust and elemental carbon mass concentration for particles with aerodynamic
686 diameters less than 10 μm, and e) skin seawater temperature from the sea snake and downwelling longwave
687 radiation.

688

689

690
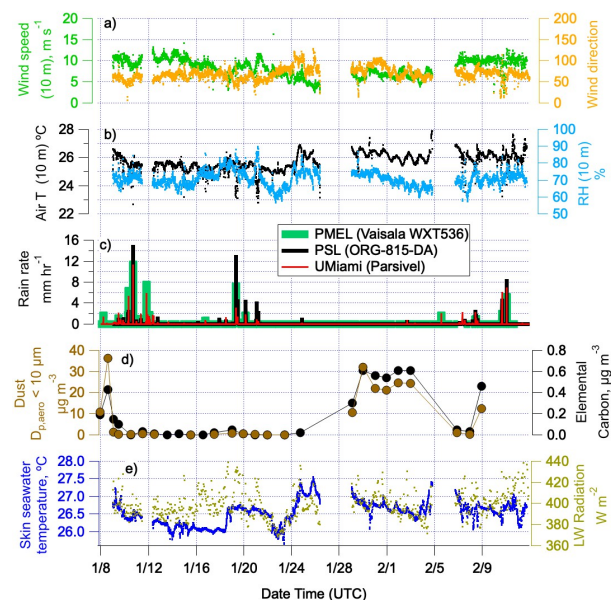
691 between Jan. 9 and 12; Jan. 19 and 21; and Feb. 8, 10, and 11 (Figure 4c). January rain events were associated with a

692 stationary front extending along 20°N from the east into Barbados. February events occurred as an Atlantic ridge

693 progressed eastward inducing strong winds and scattered showers.

694

695 One unique feature of the atmospheric conditions during ATOMIC was the occurrence of high concentrations of

696 dust in the boreal winter. Dust concentrations have long been documented to increase each summer in the Caribbean

697 due to transport from Africa (Prospero and Mayol-Bracero, 2013). A layer of warm, dry air above the marine

698 boundary, known as the Saharan Air Layer (SAL), extends from Africa to North America during the summer which

699 leads to relatively long aerosol residence times and efficient transport of dust between the two continents (Petit et

700 al., 2005;Carlson and Prospero, 1972). Factors contributing to dust transport to the Caribbean during the winter are

701 not as well understood but have been shown to correlate with the southward movement of the Intertropical

702 Convergence Zone (ITCZ) which affects near-surface northeasterly winds over North Africa (Doherty et al., 2012).

703 As a result, the SAL occurs at lower altitudes and more southern latitudes in the winter (Tsamalis et al., 2013;Liu et

704 al., 2012).

705

706 Filter measurements of particulate Al, Si, Ca, Fe, and Ti onboard the *RV Ronald H. Brown* were used to derive dust

707 concentrations (Malm et al., 1994). As shown in Fig. 4d, elevated dust concentrations were observed at the

708 beginning of Leg 1 (Jan 8 00:00 to Jan. 9 12:00) and two more times during Leg 2 (Jan. 29 12:00 to Feb. 3 19:00

709 and Feb. 9 00:00 to Feb. 11 12:00). Dust concentrations were still elevated when aerosol sampling was halted on

710 Feb. 3 and Feb. 11. Elemental carbon (EC) concentrations were enhanced during these same periods indicating

711 transport of biomass burning along with the dust. The NASA Fire Information for Resource Management System

712 (FIRMS) satellite product indicated a wide swath of fires over North Africa during January and February of 2020

713 (https://earthdata.nasa.gov/earth-observation-data/near-real-time/firms).

714

715 The ATOMIC study area was characterized by warmer skin seawater temperatures nearer to Barbados (west of

716 ~55°W) due, in part, to the North Brazil Current (NBC) that transports South Atlantic warm water along the coast of

717 Brazil and into the northern hemisphere, separating from the coast around 6° to 8°N. Occasionally the NBC curves

718 back on itself and pinches off warm eddies that move further north and into the Caribbean Sea (Fratantoni and

719 Glickson, 2002). The coolest skin seawater temperatures were encountered in the vicinity of the NTAS and MOVE

720 operations on the most northeastern portion of the cruise track between Jan. 12 and 16 (Fig. 1a and Fig. 4e). A

721 second period of low skin seawater temperatures coincided with sustained relatively low longwave downwelling

722 radiation on Jan. 22 and 23 (Fig. 4e) although causes of the low temperatures have yet to be determined.

723

724 **4. Inter-platform data comparisons**

725

726 Times when the *RV Ronald H. Brown* was in close proximity to or upwind of other sampling platforms are listed in

727 Table 3. These periods provide the potential for inter-platform comparisons for data quality checks or scientific

728 purposes. Inter-platform comparisons reported here include 1) NTAS moorings and the ship (seawater and

729 atmospheric parameters), 2) Saildrone 1064 and the ship (seawater and atmospheric parameters), 3) BCO and the

730 ship (atmospheric parameters), 4) BACO and the ship (aerosol properties), and 5) BCO, the ship, and RAAVEN

731 UAS (cloud base height). These comparisons were done to evaluate consistencies in the measurements. Resolving

732 identified inconsistencies will be the subject of future research.

733

734 **4.1. Comparison of seawater parameters**

735

736 4.1.1. Onboard RHB. No significant offsets or biases were found among the independently calibrated subsurface

737 temperature measurements onboard *RV Ronald H. Brown*. Measurements from the ship's CTD, uCTD, PSL sea

738 snake, and ship's underway thermosalinograph and thermistor were similar. After correcting for a small bias found

739 in the uCTD salinity, no significant difference was found among the different salinity measurements recorded.

740

741 4.1.2. NTAS – RHB. Four CTD casts with the ship's rosette were conducted to compare to the NTAS moorings'

742 upper ocean measurements between Jan. 12 and 15. The ship was 3 NM southwest of the NTAS-18 mooring anchor

743 on Jan. 12 and 13 and 3.8 NM northwest of the NTAS-17 mooring anchor on Jan. 15 (Table 3 and Fig. 5a). With an

744 anchor radius watch circle of ~ 2 NM for each buoy, the ship and buoys were within 0.25 to 3 NM of each other.

745 NTAS measurements of temperature and salinity at 5 depths (10, 25, 40, 55, and 70 m) are overlaid onto data from

746 the ship's CTD in Figure 5. Absolute differences (NTAS – RHB) in temperature are less than 0.1°C for all depths of

747 the three casts conducted on Jan. 12 and 13 except for the last cast during that period (Fig. 5j). For the most part, the

748 salinity comparisons show good agreement for the Jan. 12 and 13 casts with absolute differences at depths between

749 10 and 40 m being less than 0.03 (Fig.5 k). Exceptions occurred at lower depths due to strong vertical gradients.

750

751 The comparison from Jan. 15 shows significant differences for both temperature (Fig. 5j) and salinity (Fig. 5k)

752 likely due to horizontal gradients. Satellite derived sea surface salinity and SST for this day indicate that NTAS and

753 the ship were located in a frontal region with the ship in warmer and saltier surface water to the north of NTAS. The

754 sign of the absolute differences (NTAS – RHB) in temperature and salinity varied with depth. The ship's ADCP

755 revealed vertical structure in the currents consistent with the sign of observed absolute differences at the surface

756 versus lower depths.

757

758 **4.2. Comparison of atmospheric parameters**

759

760 4.2.1. NTAS – RHB

761

762 Atmospheric parameters (temperature, relative humidity, specific humidity, wind speed, pressure, rain rate, and

763 longwave downwelling radiation) measured onboard the NTAS buoys and the *RV Ronald H. Brown* were compared

764 when the platforms were within 3 NM of each other between Jan. 10 and 15 (Table 3). Measurements from NTAS-

765 17 and NTAS-18 were combined into one data set for the comparison. Based on 1-hr averaged data, 59 samples

766 were available for comparison.

767

768 Wind speed, temperature, and specific humidity from both platforms were adjusted to a height of 10 m. Absolute

769 differences (NTAS – RHB) were positive for temperature (Fig. 6a), RH (Fig. 6b), specific humidity (Fig. 6c), and

770 wind direction (Fig. 6d). These differences, however, were within either reported accuracies of the instrumentation

771 or within the range reported for a previous 24-hr *RV Ronald H. Brown* – Stratus 4 buoy comparison (Colbo and

772   Weller, 2009). Absolute differences (NTAS – RHB) were negative for wind speed, pressure, rain rate, and longwave

773   downwelling radiation although all differences were within accuracies of the instrumentation or within the range

774   reported by Colbo and Weller (2009).

775

776

777

778

779 **Figure 5.** Comparison of upper ocean measured parameters from the NTAS 18 mooring and the *RV Ronald H.*
780 *Brown* on Jan. 12, 13, and 15 with a) location of NTAS-18 mooring anchor. The NTAS buoys were about 2 NM
781 downwind (SW) of the anchor so the CTD and mooring measurements were within 0.5 to 3 NM of each other. Also
782 shown are b – e) temperature, f – i) salinity, and j – k) absolute differences and root mean square differences (rmsd)
783 for temperature and salinity, respectively. Number of samples = 4.
784
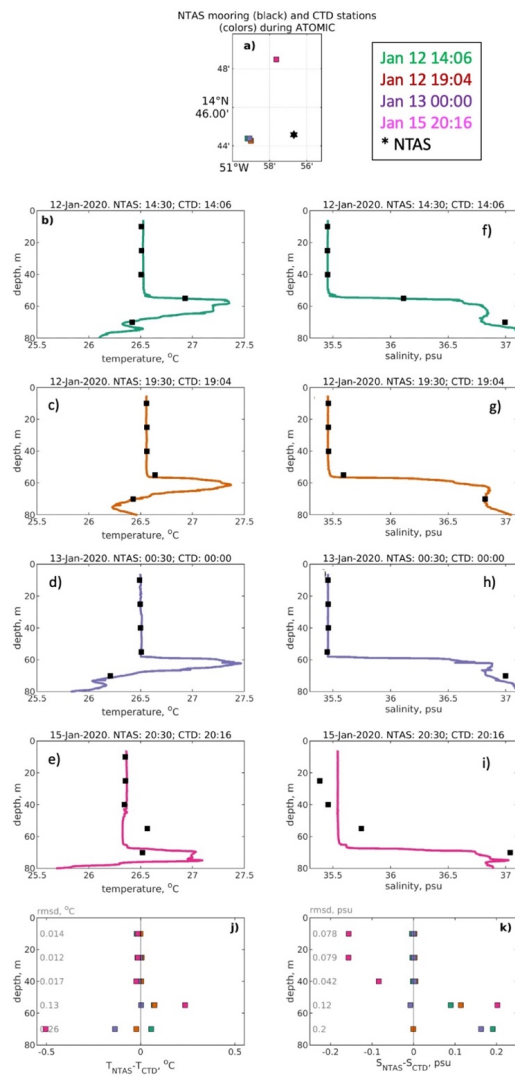
785
786

787 **Figure 6.** Comparison of meteorological parameters measured onboard the NTAS buoy and the *RV Ronald H.*
788 *Brown* (RHB) when the platforms were between 0.25 and 3 NM apart between Jan. 10 and Jan. 15 including a)
789 atmospheric temperature (10 m), b) relative humidity (10 m), c) specific humidity (10 m), d) wind direction, e) wind
790 speed (10 m), f) atmospheric pressure (10 m), g) rain rate, and h) longwave downwelling radiation. The averaged of
791 absolute differences (NTAS – RHB) and root mean square differences (rmsd) are reported in the inset table. Number
792 of samples based on 1 hr averaged data = 59.
793
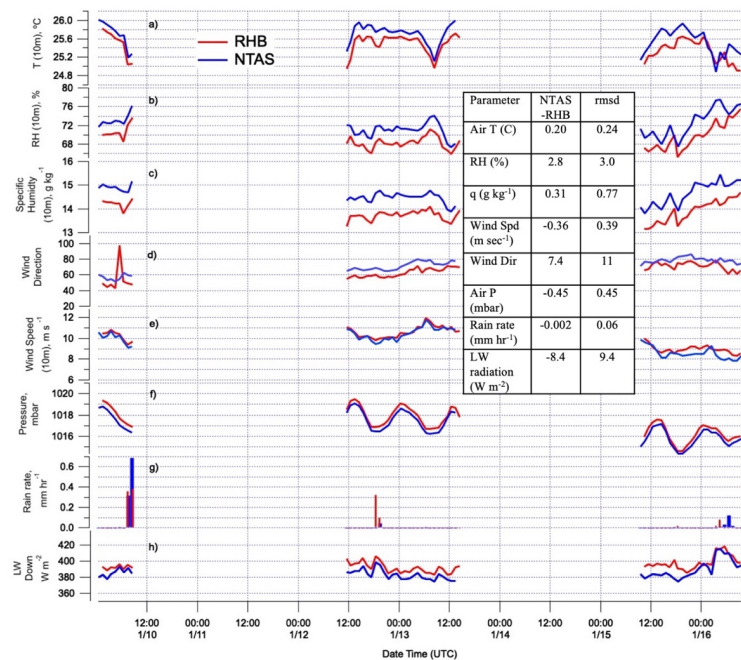
794
795
796   4.2.2. BCO – RHB
797

798   The Barbados Cloud Observatory (BCO) is located at Deebles Point on the eastern coast of Barbados. Atmospheric

799   parameters (temperature, RH, wind direction and speed, pressure, and rain rate) were compared between BCO and

800   the ship during the period the ship was 20 NM east and upwind of the observatory (Jan. 24 18:20 to Jan. 25 23:40)

801   (Table 3). BCO meteorological sensors were located at 30 m.a.s.l. and were not adjusted to a height of 10 m due to

802   uncertainties in adjusting overland measurements (BC0) with surface fluxes from the *RV Ronald H. Brown.* Based

803   on 10-min averaged data, 177 samples were available for comparison.

804

805   The average of the absolute difference (BCO – RHB) in temperature over the entire period was larger than

806   instrumental accuracies (Fig. 7a). The largest difference was observed after 12:00 UTC (08:00 local) indicating

808 relatively more warming of the sensor and/or atmosphere at BCO due to diurnal heating of the land surface. Even
809 with differences in temperature, RH values from the two platforms agreed well with the exception of the end of the
810 period. The ship observed an abrupt change in temperature and RH on Jan. 25 at 19:30 (Fig. 7a,b) suggesting that
811 the platforms were in different air masses. Wind direction agreed well between platforms (Fig. 7c) but the average
812 of the absolute differences (BCO – RHB) in wind speed (Fig. 7d) and pressure (Fig. 7e) were larger than
813 instrumental uncertainties. One rain event occurred during the comparison. It was observed on Jan. 24 on the ship
814 and 30 minutes later at BCO with observed rain rates of 1.2 and 3.5 mm hr^{-1}, respectively (Fig. 7f).
815
816 **Figure 7.** Meteorological parameters measured during the *RV Ronald H. Brown* (RHB) and the Barbados Cloud
817 Observatory (BCO) comparison (Jan. 24 18:20 to Jan. 25 23:40) when RHB was 20 NM due east of BCO.
818 Parameters include a) atmospheric temperature, b) relative humidity (RH), wind direction, wind speed, atmospheric
819 pressure, and rain rate. The average of the absolute differences (BCO – RHB) and root mean square differences
820 (rmsd) are reported in the inset table. BCO meteorological sensors were located at 30 m.a.s.l. and were not adjusted
821 to a height of 10 m. Number of samples based on 10 minute averaged data = 177.
822

Parameter	BCO – RHB	rmsd
Air T (C)	0.53	0.74
RH (%)	-0.39	3.4
Wind Dir	5.5	14
Wind Spd (m sec^{-1})	-2.0	2.3
Air P (mbar)	-2.6	2.6
Rain rate (mm hr^{-1})	2.3*	

*n = 1 (Jan. 20 event with BCO shifted 0.5 hr earlier)
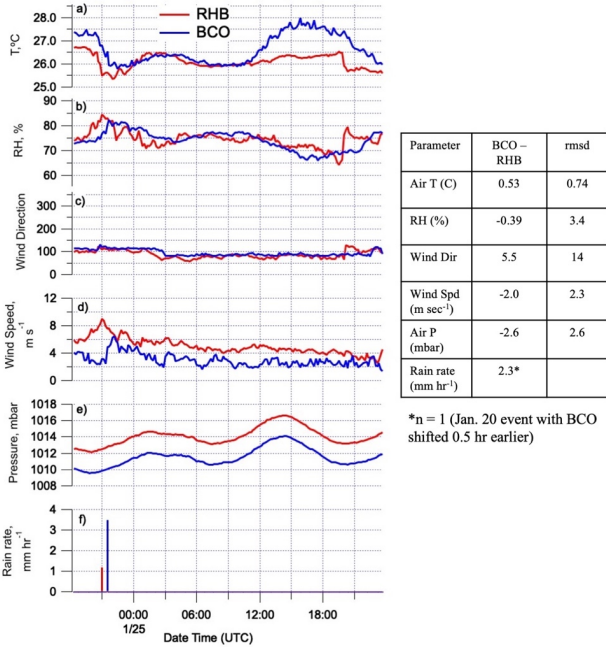
823
824
825 4.2.3. SD1064 – RHB
826

827 Saildrone 1064 and the *RV Ronald H. Brown* were within 0.7 to 3.6 NM of each other between Feb. 8 and 10.

828 Based on 10 min averaged data, 663 samples were available for the comparison. Air temperature, RH, and wind

829 speed adjusted to 10 m were used for the comparison. Skin seawater temperature was measured at a depth of 0.05 m

830 on the Saildrone and from the ship's Sea Snake. On average, skin seawater temperature agreed within 0.01°C,

831 atmospheric temperature within 0.12 °C, and RH within 1.9%. – all within the uncertainty of the measurements or

832 within the agreement observed between the NTAS buoy and the ship (see Sect. 4.2.1.) (Fig. 8a, b, c). At the end of

833 the comparison, ship measured seawater temperature at 0.05 m decreased, atmospheric temperature decreased, and

834 RH increased while Saildrone observed parameters remained steady even though the platforms were within 0.8 NM

835 of each other. These differences indicate the fine scale nature of structural differences in surface oceanic and lower

836 atmospheric conditions.

837

838 On average, agreement for wind direction and wind speed was not within instrumental uncertainties or the

839 agreement observed between the NTAS buoy and the ship due to spikes in the ship's measurements not observed by

840 the Saildrone (Fig. 8d, e). Atmospheric pressure agreed well with an absolute difference (SD0164 – RHB) of -0.27

841 mbar (Fig. 8f). The absolute difference in downward long wave radiation (SD0164 – RHB) was 4.4 W m^{-2},

842 indicating a systemic offset (Fig. 8g).

843

844

847 **Figure 8.** Comparison of parameters measured onboard Saildrone 1064 (SD1064) and *RV Ronald. H. Brown* (RHB)
848 when the platforms were within 0.7 to 3.6 NM of each other between Feb. 8 and 10. Parameters include a) SST (SD
849 at -0.05 m and RHB Sea Snake), b) air temperature (10 m), c) RH (10 m), d) wind direction, e) wind speed (10 m),
850 f) atmospheric pressure (10 m), and g) longwave downwelling radiation. Absolute differences (SD1064 – RHB) and
851 root mean square differences (rmsd) are reported in the inset table. Number of samples based on 10 min averaged
852 data = 663.

Parameter	SD1064 – RHB	rmsd
SST (C)	0.01	0.19
Air T (C)	0.12	0.45
RH (%)	1.9	3.6
Wind Spd (m sec⁻¹)	0.55	1.5
Wind Dir (m sec⁻¹)	13	2.2
Air P (mbar)	-0.27	0.49
LW Radiation (W m⁻²)	4.4	14

853
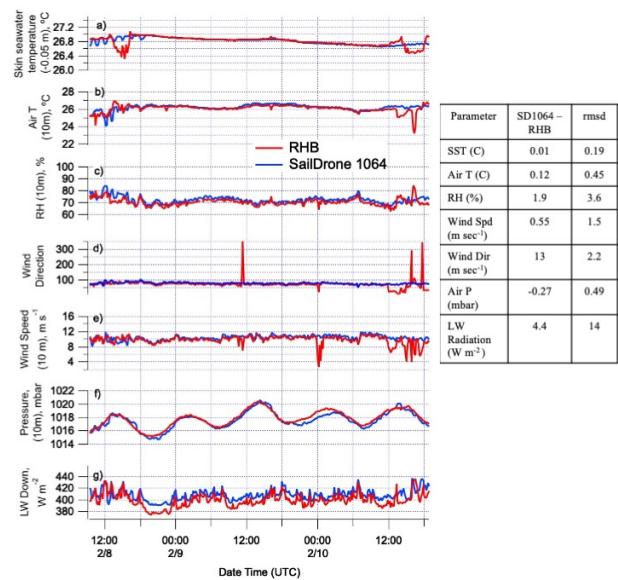
854 **4.3. Comparison of aerosol and cloud parameters**

855

856 4.3.1. BACO – RHB – aerosol parameters

857

858 The Barbados Atmospheric Chemistry Observatory (BACO) is located at Ragged Point, 400 m across a cove from
859 BCO. Total particle number concentration (CN), cloud condensation nuclei (CCN) concentration at 0.4%
860 supersaturation, and particle number size distributions were compared between BACO and the ship when the ship
861 was 20 NM east and upwind of BACO (Jan. 24 18:20 to Jan. 25 23:40) (Table 3). Details on the *RV Ronald H.*
862 *Brown* aerosol measurements are shown in Table 5 and details on CCN calibration and measurements are provided
863 in Quinn et al. (2019). Details on BACO CCN calibrations and measurements are provided in Pöhlker et al. (2018).
864

865 CN and CCN concentrations are shown in Fig. 9 from the time when BACO measurements began (Jan. 22 00:16) to
866 when the ship's measurements ended (Feb. 9 20:20). Based on CN concentrations below 300 cm^{-3}, both platforms
867 encountered clean marine conditions until ~Jan. 29 at 12:00. Subsequent enhanced concentrations of both CN and
868 CCN correspond to periods when dust and biomass burning reached the study area after transport from Africa (Fig.
869 4d) as observed in related earlier studies (Wex et al., 2016). The coherence of CN and CCN between the platforms,
870 even when separated by 4 degrees of longitude, indicates a broadscale dust event.
871

872 **Figure 9.** Aerosol parameters measured onboard the *RV Ronald H. Brown* (RHB) and at Barbados Atmospheric
873 Chemistry Observatory (BACO) for the period of overlapping measurements. The rectangle indicates the
874 comparison period (Jan. 24 18:20 to Jan. 25 23:40) when RHB was 20 NM due east of BACO. Parameters include a)
875 total particle number condensation (CN) and b) cloud condensation nuclei concentration (CCN) measured at 0.4%
876 supersaturation. The average of the absolute differences (BACO – RHB) and root mean square differences (rmsd)
877 for the comparison period are reported in the inset table. Number of samples = 5.

878
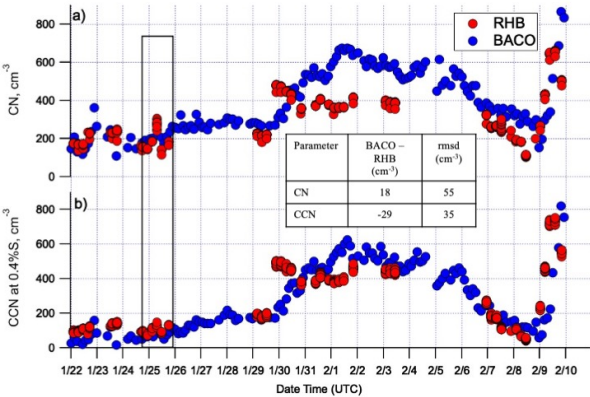
881 The comparison when the ship was 20 NM upwind of BACO is indicated by the rectangle in Fig. 9. CCN

882 concentrations were compared at a single supersaturation (S = 0.4%) which limited the number of samples to 5. The

883 absolute difference (BACO – RHB) was 18 cm^{-3} for CN, which is less than 10% of the average CN concentration

884 during the comparison period and less than measurement uncertainties (Rose et al., 2008) (Fig. 9a). The difference

885 for CCN was -29 cm^{-3} indicating the ship observed more CCN at S = 0.4% than BACO (Fig. 9b). However, this

886 difference is within the combined uncertainty of 30% for mono- and polydisperse CCN measurements.

887

888 Shipboard and BACO size distributions averaged over the length of the comparison were bimodal with Aitken

889 modal diameters of ~40 nm for both the ship and BACO and 130 and 170 nm for the accumulation mode for the

890 ship and BACO, respectively (Fig. 10). Differences in magnitude could be due to instrumental issues or local

891 aerosol sources at BACO.

892

893 **Figure 10.** Comparison of aerosol number size distribution measured onboard the *RV Ronald H. Brown* (RHB) and
894 at the Barbados Atmospheric Chemistry Observatory (BACO) during the comparison period (Jan. 24 18:20 – Jan. 25
895 23:40) when RHB was 20 NM to the east of BACO.

896

897
898
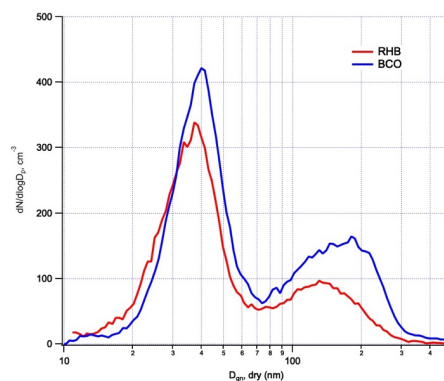
899 4.3.2. BCO – RHB – cloud base height

900

901 Cloud base height (CBH) was derived from three different measurements onboard the *RV Ronald H. Brown* – LCL

902 calculated from the stitched together RHB – BCO radiosonde record (equation 1), the ceilometer, and the microDop

903 lidar (Fig. 11a). Fifth and 10th percentile values of the lowest cloud scattered return were averaged over 10 min

904 intervals of the ceilometer and lidar data, respectively. The choice of percentile levels was tested to reduce inclusion

905 of scattering at the surface made by rain and scattering aloft from horizontally-sheared cloud edges. Higher altitude

906 ceilometer and lidar values that remain in this time series are not representative of cloud base due to the presence

907 and scattering by sheared edges or detrained portions of clouds that are separated horizontally from the locations of

910 cloud base. Dilution of surface parcels with drier air could also contribute to rising heights of the cloud base. Lowest

911 values from both the ceilometer and lidar track well with the LCL values derived from the radiosondes.

912 **Figure 11.** Comparison of Cloud Base Height (CBH) for a) legs 1 and 2 onboard *RV Ronald H. Brown* (RHB) based
913 on LCL calculated from the stitched together RHB – BCO radiosonde record (equation 1), the ceilometer, and the
914 Doppler lidar and b) for the RHB – BCO comparison period (Jan. 24 18:20 – Jan. 25 23:40) based on the BCO
915 ceilometer, LCL from BCO radiosondes, the RHB ceilometer and microDop lidar, and the RAAVEN UAS flown
916 from Morgan Lewis (30 km north of BCO). Locations of the RAAVEN launch site, BCO, and RHB are shown in c).
917 The average of the absolute differences and root mean square differences (rmds) are shown in the table inset relative
918 to the RHB lidar-derived CBH. N indicates number of samples used in the comparison. *rmsd for RHB ceilometer –
919 RHB microDop lidar with CBH greater than 1000 m removed from comparison.
920

Comparison to RHB lidar	Absolute difference (m)	rmsd (m)	N
RHB cruise Legs 1 and 2			
RHB-BCO LCL from sondes	-137	15	197
RHB ceil	0.66	360 73*	3139
BCO comparison period			
BCO LCL from sondes	-37	88	6
RHB ceil	68	81	91
BCO ceilometer	35	200	56
RAAVEN	110	32	6

921

922
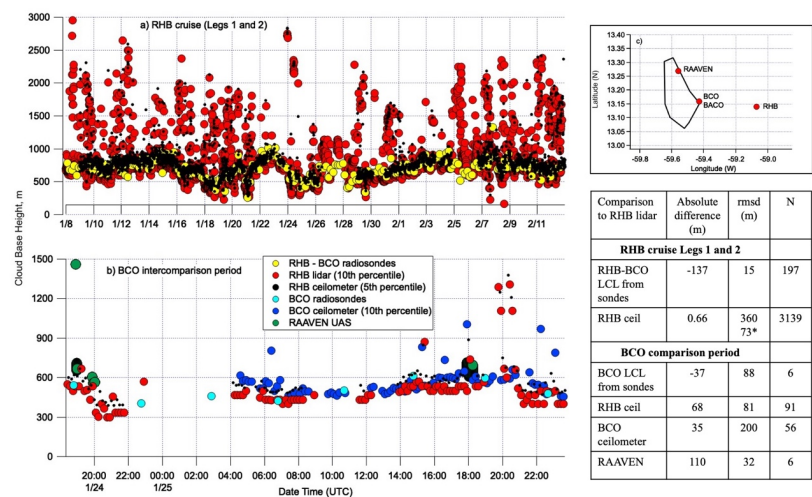
923 On average, the absolute difference between the LCL and lidar values (RHB-BCO LCL – RHB lidar) is -137 m due

924 to lidar scattering off of slightly higher altitude clouds. On average, the absolute difference between the RHB

925 ceilometer and microDop lidar (RHB ceilometer – RHB lidar) is 0.66 m indicating good agreement while the rmsd

926 value of 360 m reveals larger point to point differences. If CBHs from the ship's ceilometer and microDop lidar are

927 limited to values less than 1000 m, rmsd decreases to 73 m.

928

929 For the BCO comparison period (Jan. 24 18:20 – Jan. 25 23:40), CBHs were compared from the ship's ceilometer

930 and microDop lidar, BCO's ceilometer and LCLs from radiosondes, and the RAAVEN UAS miniFlux payload (Fig.

931 11b). The RAAVEN UAS flew from the eastern side of Barbados, 30 km north of BCO. Locations of the RAAVEN

932 launch site, BCO, and ship during the comparison are shown in Fig. 11c. Absolute differences in average values

933 between the BCO ceilometer and RHB microDop lidar (BCO ceilometer – RHB microDop lidar) and BCO LCLs

934 and RHB microDop lidar (BCO LCL – RHB microDop lidar) are around 35 m or 7% of the average sonde-derived

935   CBH. The absolute difference in average values between the RHB ceilometer and RHB microDop lidar (RHB
936   ceilometer – RHB microDop lidar) is slightly higher at 68 m. RAAVEN values are slightly higher with an absolute
937   difference (RAAVEN miniFlux – RHB microDop lidar) of 110 m. Differences could be related to finer-scale
938   horizontal and vertical variability in boundary layer structure not readily-resolved by the measurements.
939
940   **5. Data availability**
941
942   All ATOMIC data sets discussed are publicly available at the NOAA PSL ATOMIC ftp server
943   (ftp://ftp2.psl.noaa.gov/Projects/ATOMIC/data/) (Quinn et al., 2020). Point of contact information and links to the
944   data sets are provided in Table 11. In addition, data have been submitted to NOAA's National Center for
945   Environmental Information (https://www.ncei.noaa.gov/) for Digital Object Identifiers (DOIs). The data will be
946   permanently and publicly available on the PSL ftp server and NCEI.
947
948   A readme file (README_ATOMIC_DATA.pdf) is available at ftp://ftp2.psl.noaa.gov/Projects/ATOMIC/data/
949   which describes the file structure of the ATOMIC folder and the content of the single files.
950
951   All of the datasets included in the discussion have been quality-controlled based on procedures implemented by the
952   individual research teams. Versioning also is based on protocols put in place by individual research teams. Details
953   can be found in the references listed in Table 11. Data are CF compliant. File name structure is:
954
955   <campaign_id>_<project_id>_<platform_id>_<instrument_id>_<variable_id>_<time_id>_<version_id>.nc.
956
957   An example for data collected from the ceilometer on the *RV Ronald H. Brown* is as follows. The name of the data
958   and link are:
959
960   EUREC4A_ATOMIC_RonBrown_Ceilometer_10min_20200109_20200212_v1.0.nc.
961
962   Metadata are embedded in the individual .nc files for each data set.
963
964

965 **Table 11**. Summary of data sets, links to data sets, point of contact information, and references for data collected
966 onboard the *RV Ronald H. Brown*, NTAS, Wave Gliders, SWIFTs, NOAA and NASA operated Saildrones, and
967 RAAVEN UAS during ATOMIC. Links in the table are for the ftp server
968 (ftp://ftp2.psl.noaa.gov/Projects/ATOMIC/data/). (Quinn et al., 2020). Data have been submitted to NOAA's
969 National Center for Environmental Information (https://www.ncei.noaa.gov/) for Digital Object Identifiers (DOIs)
970 and for permanent archiving. The data will be permanently and publicly available on the PSL ftp server, and NCEI.
971

Platform	Data set	Data Link (preliminary FTP site location while NCEI DOIs are still being minted)	Point of Contact	Reference
All	ATOMIC	ftp://ftp2.psl.noaa.gov/Projects/ATOMIC/data/	elizabeth.thompson@noaa.gov	Zuidema (2020)
RHB	Air-sea fluxes, ship navigation/location information, meteorological parameters, solar and infrared radiation, rain rate, subskin seawater T, skin seawater T (NOAA PSL)	ftp://ftp2.psl.noaa.gov/Projects/ATOMIC/data/rhb/met_sea_flux_nav/	elizabeth.thompson@noaa.gov	Fairall et al. (1997);Fairall et al. (2003);Edson et al. (2013)
	ROSR skin seawater T (NOAA PSL)	ftp://ftp2.psl.noaa.gov/Projects/ATOMIC/data/rhb/ROSR/	elizabeth.thompson@noaa.gov	
	Ceilometer (NOAA PSL)	ftp://ftp2.psl.noaa.gov/Projects/ATOMIC/data/rhb/ceilometer/	elizabeth.thompson@noaa.gov	
	Disdrometer (rain rate, drop number, equivalent radar reflectivity) (U Miami)	ftp://ftp2.psl.noaa.gov/Projects/ATOMIC/data/rhb/disdrometer/	pzuidema@rsmas.miami.edu	(Löffler-Mang and Joss, 2000)
	W-band radar (U Miami in partnership with NOAA PSL)	ftp://ftp2.psl.noaa.gov/Projects/ATOMIC/data/rhb/W-band-radar/	pzuidema@rsmas.miami.edu elizabeth.thompson@noaa.gov	
	Sky camera (U Miami)	https://www.dropbox.com/sh/zejurecda70bilq/AABlLWgrEv1MDZ07yIE5TgWWa?dl=0	pzuidema@rsmas.miami.edu	
	M-AERI skin seawater T, air humidity and temperature (U Miami)	ftp://ftp2.psl.noaa.gov/Projects/ATOMIC/data/rhb/M-AERI/	pzuidema@rsmas.miami.edu gszczodrak@rsmas.miami.edu	Szczodrak et al. (2007)
	Doppler lidar (NOAA CSL)	ftp://ftp2.psl.noaa.gov/Projects/ATOMIC/data/rhb/doppler_lidar/	alan.brewer@noaa.gov	Schroeder et al. (2020)
	Picarro water vapor isotopes (OSU/NCAR)	ftp://ftp2.psl.noaa.gov/Projects/ATOMIC/data/rhb/Picarro/	david.noone@auckland.ac.nz	
	Picarro seawater isotopes	ftp://ftp2.psl.noaa.gov/Projects/ATOMIC/data/rhb/seawater_isotopes/	david.noone@auckland.ac.nz	
	Meteorological and aerosol properties (NOAA PMEL)	ftp://ftp2.psl.noaa.gov/Projects/ATOMIC/data/rhb/atmos-chem/	derek.coffman@noaa.gov	Bates et al. (2002)
	Radiosondes (OSU)	https://doi.org/10.5194/essd-2020-174	simon.deszoeke@oregonstate.edu	Stephan et al. (2020)
	Underway CTD, uCTD (APL-UW)	ftp://ftp2.psl.noaa.gov/Projects/ATOMIC/data/rhb/UCTD/	kdrushka@apl.uw.edu	Mojica and Gaube (2020)
	Ship rosette CTD (APL-UW)	ftp://ftp2.psl.noaa.gov/Projects/ATOMIC/data/rhb/CTD/	kdrushka@apl.uw.edu	
	Ship ADCP (APL-UW)	ftp://ftp2.psl.noaa.gov/Projects/ATOMIC/data/rhb/ADCP/	kdrushka@apl.uw.edu	
NTAS mooring	Meteorological parameters, air-sea fluxes, solar and infrared radiation; ocean currents, waves, conductivity, salinity, and temperature (WHOI)	ftp://ftp2.psl.noaa.gov/Projects/ATOMIC/data/NTAS/	aplueddemann@whoi.edu	Weller (2018)
Wave Gliders	Air-sea fluxes, meteorological parameters, radiation; ocean currents, turbulence, waves, conductivity, and temperature (APL-UW)	ftp://ftp2.psl.noaa.gov/Projects/ATOMIC/data/wavegliders/	jthomson@apl.washington.edu	Thomson and Girton (2017)
SWIFT drifter	Air-sea fluxes, meteorological parameters, radiation; ocean currents, turbulence, waves,	ftp://ftp2.psl.noaa.gov/Projects/ATOMIC/data/swift_drifters/	jthomson@apl.washington.edu	Thomson et al. (2019)

	conductivity, and temperature (APL-UW)			
Saildrones (NOAA)	Air-sea fluxes, meteorological parameters, radiation; ocean currents, waves, conductivity, and temperature (NOAA PMEL)	ftp://ftp2.psl.noaa.gov/Projects/ATOMIC/data/saildrones_noaa/	dongxiao.zhang@noaa.gov	Zhang et al. (2019)
Saildrones (NASA)	Air-sea fluxes, meteorological parameters, radiation; ocean currents, waves, conductivity, and temperature (NASA)	https://doi.org/10.5067/SDRON-ATOM0	cgentemann@faralloninstitute.org	
SVPS drifters	Meteorological and ocean parameters, wind stress (NOAA AOML)	ftp://ftp2.psl.noaa.gov/Projects/ATOMIC/data/svp-s_drifters/	greg.foltz@noaa.gov	Centurioni et al. (2015);Hormann et al. (2015)
RAAVEN miniFlux	Met parameters (Univ. Colorado)	ftp://ftp2.psl.noaa.gov/Projects/ATOMIC/data/CU-RAAVEN/	gijs.deboer@noaa.gov	de Boer et al. (2020)

973

974

975 As an example, the metadata for Cloud Base Height is:

976

977 long_name: cloud base height

978 standard_name: cloud_base_altitude

979 units: km

980 coverage_content_type: thematicClassification

981 instrument: ceilometer_instrument

982 platform: RonBrown

983 coordinates: time

984 cell_methods: time: point

985 valid_range: 0.0, 7.0

986 actual_range: 0.28, 6.86975

987 _FillValue: -9999.0

988 comment: Computed as the 5th percentile of cloud1, the height of first cloud layer detected, from 15 sec raw data

989 over this time period.

990

991

6. Summary

During ATOMIC, *in situ* and remote sensing measurements of oceanic and atmospheric properties and air-sea fluxes were made from the *RV Ronald H. Brown.* In addition, the NTAS mooring, radiosondes, SWIFTs, and Wave Gliders were deployed. Descriptions of the instrumentation onboard the ship and the deployed assets are provided along with the sampling strategy and day-to-day events. Atmospheric and oceanic conditions encountered during the cruise are described. Also detailed is how to access to all data collected. Comparisons were conducted with the NTAS moorings, Saildrone 1064, BCO, BACO, and the RAAVEN UAS. Data from inter-platform comparisons are presented to assess consistency in data sets. Resolving identified inconsistencies will be the subject of future research. The intention of the paper is to advance widespread use of the data by the ATOMIC and broader research communities.

Author contributions. P.K.Q. prepared the paper with the help of all co-authors. E.T. prepared data sets for archival on the PSL ftp server and at NCEI. D.J.C. prepared data for inclusion in the paper's figures. All authors participated in collecting and analyzing ATOMIC data.

Competing Interests. The authors declare that they have no competing interests.

Acknowledgements. We thank the crew of the *RV Ronald H. Brown* for their enthusiastic help and cooperation throughout the ATOMIC cruise and Dr. Edmund Blades and Peter Sealey for technical support at the BACO site. NOAA's Climate Variability and Predictability Program provided funding under NOAA CVP NA19OAR4310379, GC19-301, and GC19-305. The Joint Institute for the Study of the Atmosphere and Ocean (JISAO) supported this study under NOAA Cooperative Agreement NA15OAR4320063. Additional support was provided by the NOAA's Uncrewed Aircraft Systems (UAS) Program Office, NOAA's Physical Sciences Laboratory, and NOAA AOML's Physical Oceanography Division. The NTAS project is funded by the NOAA's Global Ocean Monitoring and Observing Program (CPO FundRef number 100007298), through the Cooperative Institute for the North Atlantic Region (CINAR) under Cooperative Agreement NA14OAR4320158. We would like to thank Dr. David Farrell of the Caribbean Institute for Meteorology and Hydrology (CIMH) for his assistance with the organization of this campaign and Dr. Sandy Lucas of NOAA's Climate Program Office for her efforts that made ATOMIC and related outreach programs a success. This is PMEL contribution number 5172.

1027 **References**

1028

1029 Banner, M. L., and Morison, R. P.: Refined source terms in wind wave models with explicit
1030 wave breaking prediction. Part I: Model framework and validation against field data, Ocean
1031 Modelling, 33, 177 - 189, 2010.
1032 Bates, T. S., Coffman, D. J., Covert, D. S., and Quinn, P. K.: Regional marine boundary layer
1033 aerosol size distributions in the Indian, Atlantic and Pacific Oceans: A comparison of INDOEX
1034 measurements with ACE-1, ACE-2, and Aerosols99, J. Geophys. Res. Atmos., 107,
1035 10.1029/2001JD001174, 2002.
1036 Bigorre, S. P., and Galbraith, N. R.: Sensor performance and data quality control, in: Observing
1037 the Oceans in Real Time, edited by: Venkatesan, R., Tandon, A., D'Asaro, E., and Atmanand,
1038 M. A., Springer International, 243 - 261, 2018.
1039 Bolton, D.: The Computation of Equivalent Potential Temperature, Monthly Weather Review,
1040 108, 1046 - 1053, 1980.
1041 Bony, S., Stevens, B., Frierson, D. M. W., Jakob, C., Kageyama, M., Pincus, R., Shepherd, T. G.,
1042 Sherwood, S. C., Siebesma, A. P., Sobel, A. H., Watanabe, M., and Webb, M. J.: Clouds,
1043 circulation, and climate sensitivity, Nature Geosci., 8, 261 - 268, 2015.
1044 Bony, S., Stevens, B., Ament, F., Bigorre, S., Chazette, P., Crewell, S., Delanoe, J., Emanuel, K.,
1045 Farrell, D., Flamant, C., Gross, S., Hirsch, L., Karstensen, J., Mayer, B., Nuijens, L., Ruppert, J.
1046 H., Sandu, I., Siebesma, P., Speich, S., Szczap, F., Totems, J., Vogel, R., Wendisch, M., and
1047 Wirth, M.: EUREC4A: A field campaign to elucidate the couplings between clouds, convection
1048 and circulation, Surveys in Geophysics, 38, 1529 - 1568, 2017.
1049 Carlson, T. N., and Prospero, J. M.: The large-scale movement of Saharan air outbreaks over the
1050 northern equatorial Atlantic, Journal of Applied Meteorology, 11.2, 283 - 297, 1972.
1051 Centurioni, L. R., Hörmann, V., Chao, Y., Reverdin, G., Font, J., and Lee, D.-K.: Sea surface
1052 salinity observations with Lagrangian drifters in the tropical North Atlantic during SPURS:
1053 Circulation, fluxes, and comparisons with remotely sensed salinity from Aquarius,
1054 Oceanography, 28, 96 - 105, 2015.
1055 Colbo, K., and Weller, R. A.: Accuracy of the IMET Sensor Package in the Subtropics, J Atmos
1056 Ocean Tech, 26, 1867 - 1890, 2009.
1057 de Boer, G., Calmer, R., Cox, C. J., Borenstein, S., Rhodes, M., Choate, C., Hamilton, J.,
1058 Argrow, B., and Intrieri, J.: Measurements from the University of Colorado RAAVEN
1059 Remotely-Piloted Aircraft System during ATOMIC, Earth System Science Data, in preparation,
1060 2020.
1061 Doherty, O. M., Riemer, N., and Hameed, S.: Control of Saharan mineral dust transport to
1062 Barbados in winter by the Intertropical Convergence Zone over West Africa, J. Geophys. Res.
1063 Atmos., 117, 10.1029/2012JD017767, 2012.
1064 Edson, J. B., Jampana, V., Weller, R. A., Bigorre, S., Plueddemann, A. J., and Fairall, C. W.: On
1065 the exchange of momentum over the open ocean, J Phys Oceanogr, 43, 1589 - 1610, 2013.
1066 Espy, J. P.: Essays on Meteorology, No. IV: North East Storms, Volcanoes, and Columnar
1067 Clouds, Journal of the Franklin Institute, 22, 239 - 246, 1836.
1068 Fairall, C. W., Bradley, E. F., Rogers, D. P., Edson, J. B., and Young, G. S.: Bulk
1069 parameterization of air–sea fluxes in TOGA COARE, J. Geophys. Res. Atmos., 101, 3747 -
1070 3767, 1996.
1071 Fairall, C. W., White, A. B., Edson, J. B., and Hare, J. E.: Integrated Shipboard Measurements of
1072 the Marine Boundary Layer, J Atmos Ocean Tech, 14, 338 - 359, 1997.

1073   Fairall, C. W., Bradley, E. F., Hare, J. E., Grachev, A. A., and Edson, J. B.: Bulk
1074   parameterization of air-sea fluxes: Updates and verification for the COARE algorithm, J Climate,
1075   16, 571 - 591, 2003.
1076   Fratantoni, D. M., and Glickson, D. A.: North Brazil Current Ring Generation and Evolution
1077   Observed with SeaWiFS, J Phys Oceanogr, 32, 1058 - 1074, 2002.
1078   Hormann, V., Centurioni, L. R., and Reverdin, G.: Evaluation of drifter salinities in the
1079   subtropical North Atlantic, J Atmos Ocean Tech, 32, 185 - 192, 2015.
1080   Liu, D., Wang, Y., Wang, Z., and Zhou, J.: The Three-Dimensional Structure of Transatlantic
1081   African Dust Transport: A New Perspective fom CALIPSO LIDAR Measurements, Adv
1082   Meteorol, 2012, 10.1155/2012/850704, 2012.
1083   Löffler-Mang, M., and Joss, J.: An optical disdrometer for measuring size and velocity of
1084   hydrometeors, J Atmos Ocean Tech, 17, 130 - 139, 2000.
1085   Malm, W. C., Sisler, J. F., Huffman, D., Eldred, R. A., and Cahill, T. A.: Spatial and seasonal
1086   trends in particle concentration and optical extinction in the United States, J. Geophys. Res.
1087   Atmos., 99, 1347 - 1370, 1994.
1088   Minnett, P., Knuteson, R. O., Best, F., and Osborne, B. J.: The Marine-Atmospheric Emitted
1089   Radiance Interferometer (M-AERI), a high-accuracy, sea-going infrared spectroradiometer, J
1090   Atmos Ocean Tech, 18, 94 - 1013, 2001.
1091   Mojica, K., and Gaube, P.: Estimates of mixing and mixed layer depth in the Western North
1092   Atlantic, Frontiers, submitted, 2020.
1093   Moran, K., Pezoa, S., Fairall, C. W., Williams, C., Ayers, T., Brewer, A., Szoeke, S. P. d., and
1094   Ghate, V.: A Motion-Stabilized W-Band Radar for Shipboard Observations of Marine Boundary-
1095   Layer Clouds. , Boundary Layer Meteorology, 143, 3 - 24, 2012.
1096   Petit, R. H., Legrand, M., Jankowiak, I., Molimie, J., Asselin de Beauville, C., Marion, G., and
1097   Mansot, J. L.: Transport of Saharan dust over the Caribbean islands: Study on an event, J.
1098   Geophys. Res. Atmos., 110, 10.1029/2004JD004748, 2005.
1099   Pincus, R., Fairall, C. W., Bailey, A., Chen, H., Chuang, P. Y., Boer, G. d., Feingold, G., Henze,
1100   D., Kazil, J., Kalen, Q. T., Leandro, M., Lundry, A., Moran, K., Naeher, D. A., Patel, A. J.,
1101   Pezoa, S., Popstefanija, I., Warnecke, J., and Zuidema, P.: Observations from the NOAA
1102   research aircraft during the ATOMIC field campaign, Earth System Science Data, in preparation,
1103   2020.
1104   Pöhlker, M. L., Ditas, F., Saturno, J., Klimach, T., de Angelis, I. H., Araujo, A. C., Brito, J.,
1105   Carbone, S., Cheng, Y., Chi, X., Ditz, R., Gunthe., S. S., Holanda, B. A., Kandler, K.,
1106   Kesselmeier, J., Konemann, T., Kruger, O. O., Lavric, J. V., Martin, S. T., Mikhailov, E., Moran-
1107   Zuloaga, D., Rizzo, L. V., Rose, D., Su, H., Thalman, R., Walter, D., Wang, J., Wolff, S.,
1108   Barbosa, H. M. J., Artaxo, P., Andreae, M. O., Poschl, U., and Pohlker, C.: Long-term
1109   observations of cloud condensation nuclei over the Amazon rain forest – Part 2: Variability and
1110   characteristics of biomass burning, long-range transport, and pristine rain forest aerosols, Atmos
1111   Chem Phys, 18, 10289 - 10331, 2018.
1112   Prospero, J. M., and Mayol-Bracero, O. L.: Understanding the transport and impact of African
1113   dust on the Caribbean Basin, Bulletin of the American Meteological Society, 94, 1329 - 1337,
1114   2014.
1115   Quinn, P. K., Bates, T. S., Coffman, D. J., Upchurch, L., Moore, R., Ziemba, L. D., Bell, T. G.,
1116   Saltzman, E. S., Graff, J., and Behrenfeld, M. J.: Seasonal variations in western North Atlantic
1117   remote marine aerosol properties, J. Geophys. Res. Atmos., 124, 14240 - 14261, 2019.

1118   Quinn, P. K., Thompson, E., Coffman, D. J., Baidar, S., Bariteau, L., Bates, T. S., Bigorre, S.,
1119   Brewer, A., Boer, G. d., Szoeke, S. P. d., Drushka, K., Foltz, G. R., Intrieri, J., Iyer, S., Fairall, C.
1120   W., Gaston, C. J., Jansen, F., Johnson, J. E., Krüger, O. O., Marchbanks, R. D., Moran, K.,
1121   Noone, D., Pezoa, S., Pincus, R., Plueddemann, A. J., Pöhlker, M. L., Pöschl, U., Melendez, E.
1122   Q., Royer, H. M., Szczodrak, M., Thomson, J., Upchurch, L. M., Zhang, C., Zhang, D., and
1123   Zuidema, P.: Measurements from the RV Ronald H. Brown and related platforms as part of the
1124   Atlantic Tradewind Ocean-Atmosphere Mesoscale Interaction Campaign (ATOMIC),
1125   ftp://ftp2.psl.noaa.gov/Projects/ATOMIC/data/, 2020.
1126   Rose, D., Gunthe, S. S., Mikhailov, E., Frank, G. P., Dusek, U., Andreae, M. O., and Poschl, U.:
1127   Calibration and measurement uncertainties of a continuous-flow cloud condensation nuclei
1128   ounter (DMT-CCNC): CCN activation of ammonium sulfate and sodium chloride aerosol
1129   particles in theory and experiment, Atmos Chem Phys, 8, 1153 - 1179, 2008.
1130   Schroeder, P., Brewer, W. A., Choukulkar, A., Weickmann, A., Zucker, M., Holloway, M. W.,
1131   and Sandberg, S.: A Compact, Flexible, and Robust Micropulsed Doppler Lidar, J Atmos Ocean
1132   Tech, 37, 1387 - 1402, 2020.
1133   Smirnov, A., Holben, B. N., Slutsker, I., D.M.Giles, McClain, C. R., Eck, T. F., Sakerin, S. M.,
1134   Macke, A., P.Croot, Zibordi, G., Quinn, P. K., Sciare, J., Kinne, S., Harvey, M., Smyth, T. J.,
1135   Piketh, S., Zielinski, T., Proshutinsky, A., Goes, J. I., Nelson, N. B., Larouche, P., Radionov, V.
1136   F., Goloub, P., Moorthy, K. K., Matarrese, R., Robertson, E. J., and Jourdin, F.: Maritime
1137   Aerosol Network as a component of Aerosol Robotic Network, J. Geophys. Res. Atmos., 114,
1138   D06204, doi:10.1029/2008JD011257, 2009.
1139   Stephan, C., Schnitt, S., Schulz, H., Bellenger, H., Szoeke, S. P. d., Acquistapace, C., Baier, K.,
1140   Dauhut, T., Laxenaire, R., Morfa-Avalos, Y., Person, R., Quinones-Melendez, E., Bagheri, G.,
1141   Bock, T., Daley, A., Guttler, J., Helfer, K. C., Los, S. A., Neuberger, A., Rottenbacher, J., Raeke,
1142   A., Ringel, M., Ritchel, M., Sadoulet, P., Schirmacher, I., Stolla, M. K., Wright, E., Charpentier,
1143   B., Doerenbecher, A., Wilson, R., Jansen, F., Kinne, S., Reverdin, G., Speich, S., Bony, S., and
1144   Stevens, B.: Ship- and island-based atmospheric soundings from the 2020 EUREC4A field
1145   campaign, Earth System Science Data, under review, 2020.
1146   Stevens, B., Farrell, D., Hirsch, L., Jansen, F., Nuijens, L., Serikov, I., Brugmann, B., Forde, M.,
1147   Linne, H., Lonitz, K., and Prospero, J. M.: The Barbados Cloud Observatory: Anchoring
1148   Investigations of Clouds and Circulation on the Edge of the ITCZ, Bulletin of the American
1149   Meteological Society, 97, 787 - 801, 2016.
1150   Stevens, B., Bony, S., Farrell, D., Ament, F., Blyth, A., Fairall, C. W., Karstensen, J., Quinn, P.
1151   K., Speich, S., and e.t., a.: European project ElUcidating the RolE of Cloud-Circulation Coupling
1152   in ClimAte (EUREC4A), Earth System Science Data, submitted, 2020.
1153   Szczodrak, M., Minnett, P. J., Nalli, N. R., and Feltz, W. F.: Profiling the Lower Troposphere
1154   over the Ocean with Infrared Hyperspectral Measurements of the Marine-Atmosphere Emitted
1155   Radiance Interferometer, J Atmos Ocean Tech, 24, 390 - 402,
1156   https://doi.org/10.1175/JTECH1961.1., 2007.
1157   Thomson, J.: Wave Breaking Dissipation Observed with SWIFT Drifters, J Atmos Ocean Tech,
1158   29, 1866--1882, 10.1175/JTECH-D-12-00018.1, 2012.
1159   Thomson, J., and Girton, J.: Sustained Measurements of Southern Ocean Air-Sea Coupling from
1160   a Wave Glider Autonomous Surface Vehicle, Oceanography Magazine, 30, 104-109, 2017.
1161   Thomson, J., Girton, J. B., Jha, R., and Trapani, A.: Measurements of Directional Wave Spectra
1162   and Wind Stress from a Wave Glider Autonomous Surface Vehicle, J Atmos Ocean Tech, 35,
1163   347-363, 2018.

1164 Thomson, J., Moulton, M., de Klerk, A., Talbert, J., Guerra, M., Kastner, S., Smith, M.,
1165 Schwendeman, M., Zippel, S., and Nylund, S.: A new version of the SWIFT platform for waves,
1166 currents, and turbulence in the ocean surface layer, IEEE/OES Workshop on Currents, Waves,
1167 and Turbulence Measurements, 2019,
1168 Tsamalis, C., Chedin, A., Pelon, J., and Capelle, V.: The seasonal vertical distribution of the
1169 Saharan Air Layer and its modulation by the wind, Atmos Chem Phys, 13, 11235 - 11257, 2013.
1170 Vial, J., Bony, S., Dufresne, J. L., and Roehrig, R.: Coupling between lower-tropospheric
1171 convective mixing and low-level clouds: Physical mechanisms and dependence on convection
1172 scheme, Journal of Advances in Modeling Earth Systems, 8,
1173 https://doi.org/10.1002/2016MS000740, 2016.
1174 Weller, R. A.: Observing surface meteorology and air sea fluxes, in: Observing the Oceans in
1175 Real Time, edited by: Venkatesan, R., Tandon, A., D'Asaro, E., and Atmanand, M. A., Springer
1176 International, 17 - 35, 2018.
1177 Wex, H., Dieckmann, K., Roberts, G., Conrath, T., Izaguirre, M. A., Hartmann, S., Herenz, P.,
1178 Schafer, M., Ditas, F., Schmeissner, T., Henning, S., Wehner, B., Holger-Siebert, H., and
1179 Stratmann, F.: Aerosol arriving on the Caribbean island of Barbados: physical properties and
1180 origin, Atmos Chem Phys, 16, 14107 - 14130, 2016.
1181 Whittlestone, S., and Zahorowski, W.: Baseline radon detectors for shipborad use: Development
1182 and deployment in the First Aerosol Characterization Experiment (ACE-1), J. Geophys. Res.
1183 Atmos., 103, 16743-16751, 1998.
1184 Zhang, D., Cronin, M. F., Meinig, C., Farrar, J. T., Jenkins, R., Peacock, D., Keene, J., Sutton,
1185 A., and Yang, Q.: Comparing Air-sea flux measurements from a new unmanned surface vehicle
1186 and proven platforms during the SPURS-2 Field Campaign, Oceanography, 32, 122 - 133, 2019.
1187 Zuidema, P.: Overview of ATOMIC, in preparation, 2020.
1188